Since January 2020 Elsevier has created a COVID-19 resource centre with free information in English and Mandarin on the novel coronavirus COVID-19. The COVID-19 resource centre is hosted on Elsevier Connect, the company's public news and information website.

European Journal of Medicinal Chemistry 226 (2021) 113862

Contents lists available at ScienceDirect

European Journal of Medicinal Chemistry

journal homepage: http://www.elsevier.com/locate/ejmech

Synthesis and antiviral activity of fatty acyl conjugates of remdesivir against severe acute respiratory syndrome coronavirus 2 and Ebola virus

Naglaa Salem El-Sayed [a, b, d, 1], Alexander S. Jureka [c, 1], Megan R. Edwards [c, 1], Sandeep Lohan [a, b], Caroline G. Williams [c], Patrick T. Keiser [e], Robert A. Davey [e], Jennifer Totonchy [a], Rakesh K. Tiwari [a, b, ***], Christopher F. Basler [c, **], Keykavous Parang [a, b, *]

[a] Center for Targeted Drug Delivery, Department of Biomedical and Pharmaceutical Sciences, Chapman University School of Pharmacy, Harry and Diane Rinker Health Science Campus, Irvine, CA, 92618, USA
[b] AJK Biopharmaceutical, 5270 California Ave, Irvine, CA, 92617, USA
[c] Center for Microbial Pathogenesis, Institute for Biomedical Sciences, Georgia State University, 686 Petit Science Center, Atlanta, GA, 30302, USA
[d] Cellulose & Paper Department, National Research Centre, 33 El-Bohouth St. former (El-Tahrir St.), Dokki, Giza P.O. Box, 12622, Egypt
[e] NEIDL, 620 Albany St, Boston University, Boston, MA, 02118, USA

ARTICLE INFO

Article history:
Received 25 June 2021
Received in revised form
30 August 2021
Accepted 18 September 2021
Available online 21 September 2021

Keywords:
Ebola virus
EBOV
Fatty acyl-RDV conjugates
Remdesivir
SARS-CoV-2
Structure-activity relationships (SAR)

ABSTRACT

We report here the synthesis, purification, and characterization of mono- and di-fatty acyl conjugates of remdesivir (RDV) and their *in vitro* antiviral activity against SAR-CoV-2, an Ebola virus transcription- and replication-competent virus-like particle (trVLP) system, and infectious Ebola virus. The most potent monofatty acyl conjugate was **4b,** containing a 4-oxatetradecanolyl at the 3′ position. Monofatty acyl conjugates, 3′-*O*-tetradecanoyl (**4a**) ($IC_{50(VeroE6)}$ = 2.3 μM; $IC_{50(Calu3)}$ = 0.24 μM), 3′-*O*-4-oxatetradodecanoyl (**4b**) ($IC_{50(VeroE6)}$ = 2.0 μM; $IC_{50(Calu3)}$ = 0.18 μM), and 3′-*O*-(12-ethylthiododecanoyl) (**4e**) ($IC_{50(VeroE6)}$ = 2.4 μM; $IC_{50(Calu3)}$ = 0.25 μM) derivatives exhibited less activity than RDV ($IC_{50(VeroE6)}$ = 0.85 μM; $IC_{50(Calu3)}$ = 0.06 μM) in both VeroE6 and Calu3 cells. Difatty acylation led to a significant reduction in the antiviral activity of RDV (as shown in conjugates **5a** and **5b**) against SARS-CoV-2 when compared with monofatty acylation (**3a-e** and **4a-e**). About 77.9% of **4c** remained intact after 4 h incubation with human plasma while only 47% of parent RDV was observed at the 2 h time point. The results clearly indicate the effectiveness of fatty acylation to improve the half-life of RDV. The antiviral activities of a number of monofatty acyl conjugates of RDV, such as **3b**, **3e**, and **4b**, were comparable with RDV against the Ebola trVLP system. Meanwhile, the corresponding physical mixtures of RDV and fatty acids **6a** and **6b** showed 1.6 to 2.2 times less antiviral activity than the corresponding conjugates, **4a** and **4c**, respectively, against SARS-CoV-2 in VeroE6 cells. A significant reduction in viral RNA synthesis was observed for selected compounds **3a** and **4b** consistent with the IC_{50} results. These studies indicate the potential of these compounds as long-acting antiviral agents or prodrugs of RDV.

* Corresponding author. Chapman University School of Pharmacy, Harry and Diane Rinker Health Science Campus #262, 9401 Jeronimo Road, Irvine, CA, 92618, USA.
** Corresponding author. Georgia State University, 686 Petit Science Center, Atlanta, GA, 30302, USA.
*** Corresponding author. Chapman University School of Pharmacy, Harry and Diane Rinker Health Science Campus, #263, 9401 Jeronimo Road, Irvine, CA, 92618, USA.
E-mail addresses: tiwari@chapman.edu (R.K. Tiwari), cbasler@gsu.edu (C.F. Basler), parang@chapman.edu (K. Parang).
[1] These authors contributed equally to this work.

https://doi.org/10.1016/j.ejmech.2021.113862
0223-5234/

1. Introduction

The increasing prevalence of COVID-19 is a severe public health problem affecting people globally. COVID-19 is taking a devastating toll on human lives. The latest human mortality of COVID-19 pandemic infection is 4,500,672 people, while approximately 216 million people have been infected as of August 29, 2021 [1]. Thus, there is an urgent need for safe and effective antiviral drugs against SARS-CoV-2 and other coronaviruses while also decreasing the likelihood of developing resistance mutations. However, the discovery and approval of new compounds take several years. Therefore, several existing drugs and potential drug candidates such as remdesivir (RDV, GS-5734, **1**, Scheme 1) have been considered for repurposing as COVID-19 treatments.

RDV was developed by Gilead in 2017 as a treatment for emerging viral diseases, in particular Ebola virus (EBOV) infection [2]. RDV was effective against EBOV in cell-based assays and non-human primate *in vivo* studies [3]. However, it was found to be less effective than monoclonal antibodies in a randomized controlled trial (RCT) conducted in 681 patients of acute EBOV infection where mortality with RDV was 53%, compared to 35% with MAB114 antibody and 33.5% with the triple antibody cocktail REGN-EB3 [4]. RDV has also shown promising antiviral activity against multiple variants of animal and human coronaviruses, including the highly-pathogenic Middle East respiratory syndrome coronavirus (MERS-CoV), severe acute respiratory syndrome coronavirus (SARS-CoV), and severe acute respiratory syndrome coronavirus 2 (SARS-CoV-2) [5–9].

RDV was evaluated for SARS-CoV-2 in early 2020, and randomized clinical trials found that RDV was superior to placebo in reducing the median time to recovery to 11 days vs. 15 days, respectively, in severely ill adult patients hospitalized with Covid-19 [10,11]. However, there was no significant difference in the mortality rate between drug-treated patients (7.1%) and placebo (11.9%). RDV received Emergency Use Authorization (EUA) from the United States Food and Drug Administration (FDA) in May 2020 for patients hospitalized with severe COVID-19, prompting thousands of studies to evaluate its efficacy [11]. In October 2020, RDV was approved by the FDA for use in patients of at least 12 years and 40 kg requiring hospitalization. Wang et al. reported that RDV is a potent inhibitor of SARS-CoV-2 in VeroE6 cells with an $EC_{50} = 0.77$ μM and selectivity index >129.87 [12]. Pruijssers et al. evaluated RDV in both Calu3 human lung cells ($EC_{50} = 0.28$ μM) and primary human airway epithelial cultures ($EC_{50} = 0.01$ μM). This study showed a lower potency of RDV in established human and monkey cell lines due to their diminished ability to metabolize the compound [13].

RDV (half-life 0.39 h) is an adenosine monophosphoramidate nucleotide prodrug that is converted to the active triphosphate analog (RDV-TP, half-life 24 h) that inhibits RNA-dependent RNA polymerase (RdRp) activity, resulting in diminished viral RNA replication [3,5,6,14]. For SARS-CoV-2, and other coronaviruses, the highly conserved nonstructural protein 12 (Nsp12) serves as the RdRp [15]. The primary mechanism of inhibition for viral replication by RDV involves its conversion to the active monophosphate nucleoside analog GS-441524 as a metabolite by protein kinases. GS-441524, in turn, is converted to the active nucleoside triphosphate metabolite (GS-443902), which is incorporated into nascent RNA chains by the viral RdRp, causing delayed RNA chain termination [10,16].

Our group has previously studied the impact of fatty acylation on the antiviral activity of different anti-HIV (human immunodeficiency virus) nucleoside drugs where we demonstrated that the conjugation of certain fatty acids to the anti-HIV nucleoside reverse transcriptase inhibitors (NRTIs), such as 3′-fluoro-3′-deoxythymidine (FLT, alovudine), 2′,3′-didehydro-2′,3′-dideoxythymidine (stavudine, d4T), 2′,3′-dideoxy-5-fluoro-3′-thiacytidine (emtricitabine, FTC), and (-)-2′,3′-dideoxy-3′-thiacytidine (lamivudine, 3TC) [17–21] enhanced activity against X4, R5, cell-associated, and/or multi-drug resistant strains when compared with their parent nucleosides. For example, 5′-*O*-tetradecanoyl and 5′-*O*-(12-azidododecanoyl) derivatives of 3TC were significantly more active (16–36 fold higher) against an X4 strain of HIV-1 when compared to 3TC [21]. The same pattern was observed for a 5′-*O*-tetradecanoyl derivative of FTC that exhibited 19-fold more activity than FTC against an X4 strain of HIV-1 [20]. The conjugates were also less toxic than their parent nucleoside analogs, providing a much higher selectivity index. Furthermore, the conjugates significantly enhanced the cellular uptake versus the parent analogs and corresponding physical mixtures of fatty acids and nucleosides [19–21].

In vivo studies have demonstrated that treatment of mice with a nanoformulation of a 5′-*O*-palmitoyl derivative of FTC led to complete inhibition of HIV-1 reverse transcriptase activity for up to 10 days by the myristoylated FTC as compared with the parent FTC that had no effect beyond day 1 [22]. Similar results were obtained using a 5′-*O*-myristoyl conjugate of 3TC where a long-acting nanoformulation of a fatty acyl conjugate of 3TC was shown to reduce hepatitis B virus replication in humanized mice [23]. Additionally, Creighton et al. demonstrated that fatty acid conjugation with raltegravir tuned its release pattern, hydrolysis rate, and anti-HIV activity [24]. Overall, the studies revealed that the prodrug action was dependent on the type of conjugated fatty acid and the position of the conjugation of fatty acid to the drug.

There are many examples of marketed anticancer and antiviral prodrug and/or long-acting agents, such as valrubicin, capecitabine, valacyclovir, and tenofovir alafenamide (TAF). TAF, a prodrug of tenofovir (TFV), has higher anti-HIV activity and distribution into the lymphatic system than TFV. The active metabolite, TFV diphosphate, has an intracellular half-life of 150–180 h [25]. Fatty acid conjugation has also been used to form nanosuspensions of antiretroviral drugs to improve their bioavailability [26,27]. Thus, it is logical to develop and characterize new long-acting fatty acyl RDV conjugates to potentially provide higher stability with a longer half-life that display broad-spectrum antiviral activity. Recently, Schooley et al. [28] reported the synthesis of three novel lipophilic, monophosphate of RDV nucleoside (RVn, GS-441524) prodrugs, two of which had anti-SARS-CoV-2 activity 9 to 24 times greater than that of RDV in Vero E6 cells.

The presence of a 1′-CN group on RDV and its metabolites confers high selectivity for viral RdRps compared to human polymerases. The cryo-EM structure of RDV-TP in complex with the SARS-CoV-2 RdRp (PDB: 6M71) showed residue S861 in Nsp12 sterically interacts with 1′-CN, inducing a delay in chain termination [29]. However, 2′ and 3′ residues were not involved in major interactions [16]. Thus, the 2′ and 3′ groups are opportune sites for modification to enhance RDV permeability and potency. RDV, like other conventional nucleotide and nucleoside analogs, suffers from poor oral bioavailability and limited gastrointestinal uptake [28].

We hypothesized that 2′ or 3′ fatty acyl conjugates of RDV will have different physicochemical properties from RDV, making their biological profiles and activities more suitable. Herein, we report the synthesis of fatty acyl derivatives of RDV and structural characterization of their antiviral activity against SARS-CoV-2 in VeroE6 cells and Calu3 cells. Five fatty acids, myristic acid, 12-azidododecanoic acid, 12-thioethyldodecanoic acid, 4-tetradodecanoic acid, and palmitic acid were conjugated to RDV at its 2′-*O*- and 3′-*O*-position. The fatty acid selection was based on the anti-HIV activity for the previously reported corresponding fatty acyl derivatives of AZT, FLT, d4T, 3TC, and FTC [17–21]. We

employed a unique antiviral screening assay that uses the continuous measurement of electrical resistance across a cell monolayer to simultaneously measure virus growth and compound cytotoxicity in parallel [30]. We also assessed their activity against an EBOV transcription- and replication-competent virus-like-particle (trVLP) system [31], and further tested three representative derivatives against infectious EBOV, validating the EBOV trVLP results.

2. Results and discussion

2.1. Synthesis of mono- and difatty acyl RDV conjugates

RDV (**1**) is composed of three components, the base moiety (4-aminopyrrolo[2,1-f][1,2,4]triazine), 2′,3′-dihydroxy-5-cyanotetra hydrofuran ring, and a phosphoramidate moiety. Five different fatty acids; myristic acid, palmitic acid, 4-toxatetradecanoic acid, 12-azidododecanoic acid, and 12-thioethyldodecanoic acid, in the form of acyl chloride (**2a-2e**), underwent reaction with the available reactive 2′ and 3′ hydroxyl groups of RDV (Scheme 1). The conjugation of the fatty acid to RDV was accomplished through two simple steps. First, the fatty acid was converted to its active acyl chloride form by treating the fatty acid with oxalyl chloride in dry benzene, according to the previously reported procedure [20].

In the second step, fatty acylation was performed by reacting an equimolar amount of the corresponding fatty acyl chloride with a dilute solution of RDV (**1**) in the presence of diisopropylethylamine (DIPEA) for 5–9 h to generate monofatty acyl derivatives that correspond to 2′- and 3′-fatty acyl RDV conjugates as **3a-e** and **4a-e**, respectively. The free aromatic amine of RDV has been shown to be less reactive than free 2′ and 3′-hydroxy groups [2,3]. The corresponding compounds from both series have the same molecular weight but differ in their chemical structures. Meanwhile, the use of 3 molar equivalents of fatty acyl chloride and 1 molar equivalent of RDV (**1**) yielded the 2′,3′-difatty acyl derivatives of RDV (**5a** and **5b)** (Scheme 1). Employing this conjugation plan by controlling the coupling conditions (i.e. reactant concentrations, temperature, and reaction time), we were able to control the target products and the yield. This direct coupling strategy was successful with the five fatty acyl chlorides used (**2a-e**) and reduced the number of reaction steps, time, and solvents required for purification. This is in contrast to the protection and deprotection strategies, which involve the selective protection of different functional groups with proper protecting agents, purification of the protected intermediates, coupling with a fatty acyl chloride, purification, removal of the protecting group, and purification of the final products in reduced yield.

Mono 3′-fatty acyl derivatives **4a-e** were obtained in higher yield as compared to 2′-fatty acyl derivatives **3a-e**, possibly due to the higher reactivity of the 3′-hydroxyl group than the 2′-hydroxyl group of RDV. The presence of an adjacent strong electron-withdrawing group (CN) at C-1′ in RDV reduces the nucleophilicity of the 2′-hydroxyl group; therefore, the carboxy chloride of the fatty acid tends to react more efficiently with the 3′-hydroxy group. The two fatty acyl monoconjugates were separated on semi-preparative reverse-phase high-performance liquid chromatography (RP-HPLC) and fully characterized using nuclear magnetic resonance (NMR) and mass spectroscopy (Supporting Information; See methods).

The attachment of the long-chain fatty acid analogs to RDV enhanced their lipophilicity, as shown by calculated partition coefficients (CLog P) (Table 1). Difatty acyl conjugates (**5a** and **5b**) exhibited significantly higher lipophilicity due to a large number of methylene chains as compared with a smaller number of methylene chains in monofatty acyl conjugates **3a-e** and **4a-e** (Table 1). Monopalmitoyl conjugates **3e** and **4e** were more lipophilic than monofatty acyl conjugates with shorter chain lengths, such as

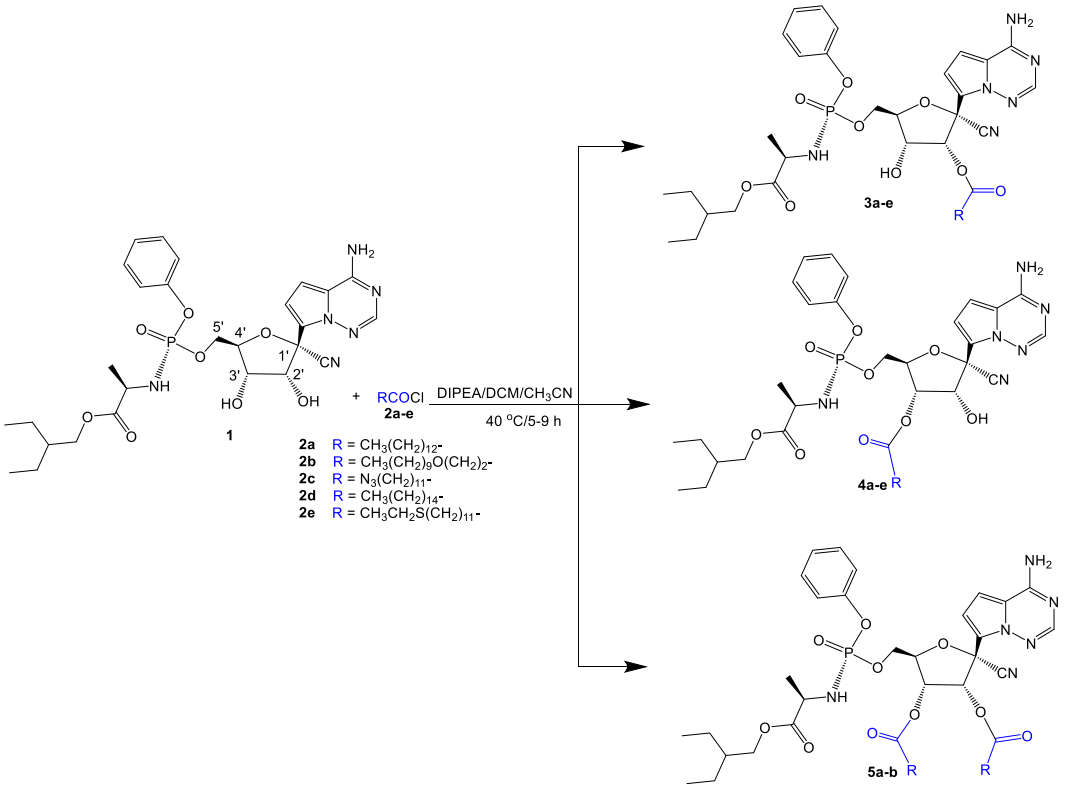

Scheme 1. Synthesis of mono- and difatty acyl RDV conjugates.

tetradecanoyl derivatives **3a** and **4a**. The higher lipophilicity is expected to improve the permeability properties in order to achieve a higher concentration of the prodrug in the infected cells. The enhanced lipophilicity of these conjugates relative to RDV should increase their ability to cross the plasma membrane. This postulate is based on the observation that increasing the lipophilicity of FTC, FLT, and 3TC improved cell permeability [19–21]. This conjugation may result in the development of antiviral prodrugs having a longer duration of action by the sustained intracellular release of active substrates at adequate concentrations and higher uptake into infected cells.

2.2. Structure elucidation using NMR spectroscopy

The 1D (^{1}H, ^{13}C, DEPT) and 2D (COSY, HSQC, and HMBC) NMR spectroscopy were used to establish the chemical structure of 3'-*O*-monosubstituted derivatives **4a-e** (Fig. 1). For example, the ^{1}H–^{1}H COSY analysis for 3′-*O*-myristoyl derivative (**4a**) showed correlations between (δ_H = 5.33 ppm, H-3′)/(δ_H = 4.56 ppm, H-4′), (δ_H = 5.33 ppm, H-3′)/(δ_H = 4.71 ppm, H-2′), (δ_H = 4.56 ppm, H-4′)/(δ_H = 4.38 ppm, H-5′), revealing that the signals with δ_H 5.33, 4.70, 4.56, and 4.42–4.29 ppm are assigned to H-3′, H-2′, H-4′, and H-5′ respectively. The ^{1}H–^{13}C HSQC correlation established that H-3′, H-2′, H-4′, and H-5′ protons with δ_H 5.33, 4.71, 4.57, and 4.41–4.30 ppm were correlated to C-3′ (δ_c 72.39 ppm), C-2′ (δ_c 75.04 ppm), C-4′ (δ_c 83.28 ppm), C-5′ (δ_c = 65.77 ppm), respectively. ^{1}H–^{13}C HMBC correlations between H-3' (δ_H 5.33 ppm) to CO fatty acyl carbonyl (δ_c=173.54 ppm) confirmed that the fatty acid was conjugated to the hydroxyl group at C-3′, and not C-2′ (Figures S27-S32, Supporting Information).

Similarly, for the 2′-O-myristoyl derivative (**3a**), ^{1}H–^{1}H COSY showed correlations between (δ_H = 4.50 ppm)/(δ_H = 4.38 ppm), (δ_H = 4.50/5.82 ppm), and (δ_H = 4.41/4.39 ppm), and revealed that the signals at δ_H 5.82, 4.54–4.44, and 4.42–4.35 ppm were assigned to H-2′, H-3′, H-5′, H-4′ and H-5″. The ^{1}H–^{13}C HSQC correlation showed that H-2′, H-3′, H-5′, H-4′, and H-5″ protons were correlated to C-2′ (δ_c 74.58 ppm), C-3′(δ_c 69.31 ppm), C-4′(δ_c 82.54 ppm), C-5′ (δ_c 65.05 ppm), respectively. The ^{1}H–^{13}C HMBC showed the correlation between H-2′ (δ_H 5.82 ppm) to the fatty acyl carbonyl (δ_c 172.75 ppm), verifying that the fatty acid was conjugated to RDV at C-2′ (Figures S1-S6, Supporting Information).

2.3. Anti-SARS-CoV-2 activity

The cytotoxicity and antiviral activity of the fatty acyl conjugates of RDV were compared among themselves and to RDV, and the physical mixture of the parent analogs with fatty acids. Screening of RDV fatty acyl conjugates for anti-SARS-CoV-2 activity was accomplished using a previously described real-time impedance-based, label-free assay that provides continuous monitoring of cell health [30].

SARS-CoV-2 induces a significant cytopathic effect (CPE) in Vero E6 cells. The assay uses the Maestro Z platform (Axion BioSystems, Atlanta, GA), an instrument that uses electrode-containing 96-well plates to continuously measure the electrical impedance across cell monolayers. As SARS-CoV-2 infection progresses and the resulting CPE becomes more severe, impedance measurements decrease over time, providing a detailed assessment of infection kinetics. Because the Maestro Z provides continuous data regarding the health of cell monolayers, compound toxicity is readily identified by significant drops in impedance measurements prior (0–24 h post-treatment) to the onset of virus-induced CPE. Vero E6 cells were pre-treated with 6-fold serial dilutions of RDV or RDV fatty acyl conjugates for 1 h and then infected with SARS-CoV-2 at an multiplicity of infection (MOI) of 0.01. Resistance measurements were recorded for 48 h post-infection (hpi). Percent inhibition was calculated at the 48 hpi time point in comparison to DMSO-treated infected and uninfected controls.

RDV fatty acyl conjugates with 50% inhibitory concentration (IC_{50}) values of $\leq$ 3 μM in Vero E6 cells were selected for further testing in the Calu3 respiratory epithelial cell line. Calu3 cells were pre-treated with 6-fold serial dilutions of RDV or RDV conjugates for 1 h and then infected with SARS-CoV-2 at an MOI of 0.01 for 48 h. At 48 hpi, supernatants were harvested, and infectious virus was quantified by immunofocus forming assay, as previously described [32,33]. Compound toxicity in Calu3 cells was assayed in parallel by CellTox green (Promega).

Table 2 shows antiviral (IC_{50}) and 50% cell cytotoxicity (CC_{50}) values of synthesized fatty acyl RDV conjugates on SARS-CoV-2 infected Vero E6 and Calu3 cell lines. Fatty acids alone, myristic acid, 4-oxatetradecanoic acid, 12-thioethydodecanoic acid, and 12-azidododecanoic acid, did not exhibit any anti-SARS-CoV-2 activity in Vero E6 cells, even at the highest concentration of 50 μM. The physical mixtures of RDV with myristic acid (**6a**) and 12-azidodecanoic acid (**6b**) exhibited IC_{50} values of 4.9 μM in the same cell line. The monofatty acyl RDV analogs showed SARS-CoV-2 antiviral activity with IC_{50} values of 2.4–4.6 μM and 0.29–3.6 μM against VeroE6 and Calu3 infected cells, respectively. The most potent monofatty acyl conjugate was **4b,** containing a 4-oxatetradecanolyl at the 3′ position, which had IC_{50} values of 2.0 μM and 0.18 μM in VeroE6 and Calu3 infected cells, respectively. RDV showed anti-SARS-CoV-2 activity with IC_{50} = 0.85 μM (VeroE6) and 0.06 μM (Calu3), which is 2.4 to 3-fold higher than the monofatty acylated RDV analog **4b**. Difatty acyl RDV conjugates **5a** and **5b** showed significantly lower anti-SARS-CoV-2 activity with IC_{50} = 31.0 μM and >50 μM, respectively, against VeroE6 infected cells. RDV demonstrated a very high selectivity index (>588 to >833) in both cell lines, as compared to all the synthesized monofatty acylated RDV conjugates (>10.9 to >208). The diminished antiviral activity of monofatty acyl conjugates of RDV can be attributed to the slow hydrolysis of the conjugates to RDV.

To confirm that the inhibition of SARS-CoV-2 by these compounds was due to inhibition of RNA synthesis, viral RNA levels from cells treated with RDV (1 μM), or a representative compound from each class of compounds (**3a** (5 μM) , **4b** (5 μM), and **5a** (45 μM)) were assessed by reverse transcription followed by quantitative PCR (qPCR). A significant reduction in viral RNA synthesis was observed for all compounds apart from disubstituted compound **5a** (Supplemental 97A), consistent with the IC_{50} results in Table 2.

The cryo-EM structure of RDV-TP in complex with the SARS-CoV-2 RdRp (PDB: 6M71) showed residue S861 sterically

Table 1
Calculated partition coefficient of fatty acyl RDV conjugates.

Compound	Fatty acyl chain	CLogP (calcd)[a]
RDV	H	1.25
3a	$CH_3(CH_2)_{12}CO$-	8.45
3b	$CH_3(CH_2)_9O(CH_2)_2CO$-	6.83
3c	$N_3(CH_2)_{11}CO$-	7.66
3d	$CH_3(CH_2)_{14}CO$-	9.51
3e	$CH_3CH_2S(CH_2)_{11}CO$-	7.54
4a	$CH_3(CH_2)_{12}CO$-	8.45
4b	$CH_3(CH_2)_9O(CH_2)_2CO$-	6.83
4c	$N_3(CH_2)_{11}CO$-	7.67
4d	$CH_3(CH_2)_{14}CO$-	9.51
4e	$CH_3CH_2S(CH_2)_{11}CO$-	7.54
5a	$CH_3(CH_2)_{12}CO$-	15.65
5b	$N_3(CH_2)_{11}CO$-	14.08

[a] Calculated partition coefficient using ChemBioDraw Ultra 20.0.

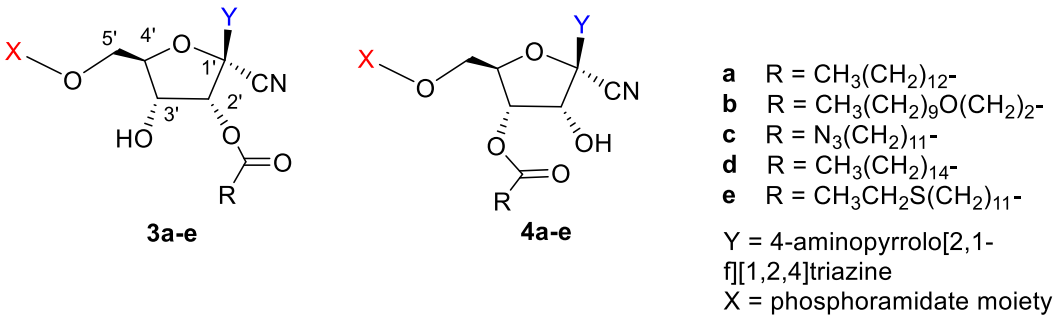

Fig. 1. General structures of fatty acyl conjugates of RDV.

Table 2
SARS-CoV-2 activity of fatty acyl RDV conjugates.[a]

Compound	VeroE6			Calu3		
	CC_{50} (μM)	IC_{50} (μM)	SI	CC_{50} (μM)	IC_{50} (μM)	SI
RDV	>50	0.85	>588	>50	0.06	>833
3a	>50	2.4	≥20.7	>50	0.29	>172
3b	>50	4.6	≥10.9	ND[b]	ND	ND
3c	>50	4.6	≥10.9	ND	ND	ND
3d	ND	ND	ND	>50	3.6	>13.9
3e	>50	3.5	≥14.2	ND	ND	ND
4a	>50	2.3	≥22.1	>50	0.24	>208
4b	>50	2.0	≥25.6	34.3	0.18	>191
4c	>50	3.0	≥16.6	>50	0.51	>98.0
4d	ND	ND	ND	>50	1.6	>32.3
4e	>50	2.4	≥20.5	>50	0.25	>200
5a	>50	31	≥1.59	ND	ND	ND
5b	>50	>50		ND	ND	ND
Myristic acid	>50	>50		ND	ND	ND
4-Oxatetradecanoic acid	>50	>50		ND	ND	ND
12-thioethyldodecanoic acid	>50	>50		ND	ND	ND
12-Azidododecanoic acid	>50	>50		ND	ND	ND
6a	>50	4.9	≥10.0	ND	ND	ND
6b	>50	4.9	≥10.2	ND	ND	ND

[a] Data reported are n = 3 in 96 well assay format.
[b] ND = not determined.

interacts with 1′-CN, inducing a delay in chain termination [16,29]. Although 2′ and 3′ residues are not involved in major interactions with the RdRp, the large substitutions at 2′ and 3′ positions may interfere with these interactions. However, it is expected that upon cellular delivery and hydrolysis to RDV, the long-acting effect of RDV is to be observed. These conjugates were designed as prodrugs to improve the physicochemical properties of RDV to be used in oral administration or as long-acting antiviral agents. Further investigation is required to determine the prodrug properties and long-acting activity of the conjugates in vivo.

2.4. Anti-EBOV activity

The anti-EBOV activity of fatty acyl RDV analogs was assessed using a transient transfection-based transcription- and replication-competent virus-like particle (trVLP) system (EBOV trVLP) (Table 3). The assay allows for modeling of the virus lifecycle at biosafety level 2 (BSL2) conditions [31]. The fatty acids alone, myristic acid, 4-oxatetradecanoic acid, 12-thioethydodecanoic acid, and 12-azidododecanoic acid, demonstrated no inhibitory activity against the EBOV trVLP. The physical mixtures of RDV with myristic acid (**6a**) and 12-azidodecanoic acid (**6b**) exhibited IC_{50} values of 0.13 and 0.09 μM, respectively. RDV and monofatty acylated RVD conjugate (**3a**, **3b**, **3c**, **3e**, **4a**, **4b**, **4c**, and **4e**) showed comparable EBOV trVLP activity with IC_{50} = 0.16–0.71 μM. However, the selectivity index for RDV was generally higher than the monofatty acylated RDV conjugates. Difatty acyl RVD conjugates showed weaker anti-EBOV trVLP activity, similar to SARS-CoV-2. To validate the compound antiviral activity identified by the EBOV trVLP assay, we further tested three of the derivatives against infectious EBOV. While RDV exhibited approximately 3-fold lower activity against infectious EBOV, relative to the EBOV trVLP assay, compound **3c** exhibited approximately 2.6-fold enhanced activity. Compound **4b** that exhibited the highest anti-SARS-CoV-2 activity among all the fatty acyl conjugates was found to be also the most potent compound against EBOV trVLP and showed comparable activity with RDV.

To confirm that the inhibition of the EBOV trVLP by these compounds was due to inhibition of RNA synthesis, viral RNA levels from cells treated with RDV (1 μM), or a representative compound from each class of compounds (**3a** (5 μM), **4b** (5 μM), and **5b** (45 μM)), were assessed by qPCR. A significant reduction in viral RNA synthesis was observed for all compounds apart from disubstituted compound **5b** (Supplemental 97B), consistent with the IC_{50} results in Table 3. Compound **5b**, which showed no inhibitory activity in the EBOV trVLP assay, was also inactive against infectious EBOV at the concentrations tested.

Table 3
The activity of fatty acyl RDV conjugates against Ebola trVLP and wild type EBOV.[a]

Compound		EBOV trVLP		Ce-FF		EBOV[c]
	CC_{50} (μM)	IC_{50} (μM)	SI	IC_{50} (μM)	SI	IC_{50} (μM)
RDV	>50	0.32	>156	24	>2.08	1.0
3a	>50	0.67	>74.6	>50		
3b	15	0.30	50.0	36	0.417	ND[b]
3c	27	0.50	54.0	>50		0.19
3d	>50	7.2	>6.94	>50		
3e	41	0.25	164	29	1.41	ND
4a	>50	0.71	>70.4	>50		
4b	7.4	0.16	46.3	14	0.529	ND
4c	20	0.45	44.4	>50		0.83
4d	>50	2.9	>17.2	>50		ND
4e	23	0.28	82.1	>50		ND
5a	>50	12.1	>4.13	>50		ND
5b	>50	>50		>50		>5.0
Myristic acid	>50	>50	>50	>50		
4-Oxatetradecanoic acid	>50	>50	>50	>50		
12-Thioethyldodecanoic acid	>50	>50	>50	>50		
12-Azidododecanoic acid	>50	>50	>50	>50		
6a	25.1	0.13	193	25.9	0.969	ND
6b	44	0.09	489	25	1.76	ND

[a] Data reported are n = 3 in 96 well assay format.
[b] ND = not determined.
[c] Data reported are n = 2.

2.5. Plasma stability

To analyze the stability imparted by fatty acylation of the parent compound, we determined the percentage digestion of RDV and one of the lead fatty acyl derivatives of RDV (**4c**) in the presence of human plasma and analyzed the data using high resolution Liquid Chromatography Quadrupole Time-Of-Flight mass spectrometry (LC-QTOF-MS) (Supporting Information, Figures S93-S96). Data are represented in the form of percentage degradation of test compound against time by measuring area under the curve in extracted ion chromatogram (EIC, Fig. 2). For RDV, around 13% degradation was observed after 1 h. However, only 47% RDV was observed at the 2 h time point. However, no degradation was observed after 2 h incubation for **4c**, and the parent compound remained intact by 77.9% after 4 h incubation. The results clearly indicate the significant effectiveness of fatty acylation to improve the half-life of the compound.

For RDV, approximately 22.2% of the active triphosphate metabolite of remdesivir (RDV-triphosphate) was observed at the 12 h time point, which was further increased to 26.3% at 24 h. Similarly, 11.3%, 10.04%, and 19.01% of the active triphosphate metabolite of **4c** were observed at 8 h, 12 h, and 24 h, respectively. Further studies will be conducted in the future to determine the outcome of the triphosphate metabolite of **4c** and the effect of the fatty acyl chain on its antiviral activity. However, these studies show that the metabolism of these compounds occurs through phosphorylation.

3. Conclusion

The modification of existing nucleoside analogs with fatty acids has been previously demonstrated to improve antiviral activity through a variety of mechanisms, including increasing their bioavailability and half-life. This suggests a mechanism by which the antiviral activity of RDV may be further improved. In this study, we demonstrate that controlled fatty acylation of RDV results in two structural isomers of 2′ and 3′ fatty acyl RDV derivatives. The yield of 3′-fatty acyl RDV was higher than 2′-fatty acyl RDV due to the 3′-hydroxyl groups of RDV seeming to be more reactive than the 2′-hydroxyl group. Further, the ratio of the fatty acid and RDV controlled the formation of products (mono and/or diconjugates).

To assess the antiviral activity of the new fatty acyl conjugates, we evaluated them against SARS-COV-2, an EBOV trVLP system, and infectious EBOV. The higher lipophilicity of the new conjugates was expected to improve the permeability properties of the compounds, allowing the prodrug to achieve a higher concentration in the infected cells, relative to RDV. This effect was previously observed when increasing the lipophilicity of FTC, FLT, and 3TC improved cell permeability, suggesting that this conjugation may result in the development of antiviral prodrugs having a longer duration of action by the sustained intracellular release of active substrates at adequate concentrations and higher uptake into infected cells [19–21]. Most monofatty acyl derivatives of RDV demonstrated IC_{50} values against SARS-CoV-2 that were slightly decreased relative to RDV. This may be attributable to slow hydrolysis of the conjugates to RDV. Against the EBOV trVLP and infectious EBOV, a number of the monofatty acyl conjugates had IC_{50}s similar to that of RDV.

Overall, these data together indicate that RDV can be modified with fatty acids at positions 2′ or 3′, without demonstrating a significant loss of antiviral activity in cell culture against SARS-CoV-2 and EBOV while generating long-acting effect *in vitro*. Future studies will determine if these modifications result in greater long-acting effect, bioavailability, and stability in animal models.

4. Experimental section

4.1. Materials

Compound **1** (RDV) was purchased from Hangzhou Molcore Biopharmatech Co., Ltd (Hangzhou, China). 12-Bromododecanoic acid, 2-ethanethiol, sodium azide, and oxalyl chloride were purchased from MilliporeSigma (USA). All the other reagents, including solvents, were purchased from Fisher Scientific (USA). The final products were purified on a Phenomenex Gemini 10 μm ODS reversed-phase column (2.1 × 25 cm) with semi-preparative Shimadzu HPLC system using a gradient system at a constant flow rate of 7 mL/min for derivatives **3a-e** and **4a-e**, and 9 mL/min for products **5a** and **5b**.

The purity of the compounds was confirmed by using a Shimadzu analytical HPLC system on a C18 column (Phenomenex Synergi™ 4 μm Hydro-RP 80 Å, LC Column 250 × 4.6 mm) using a

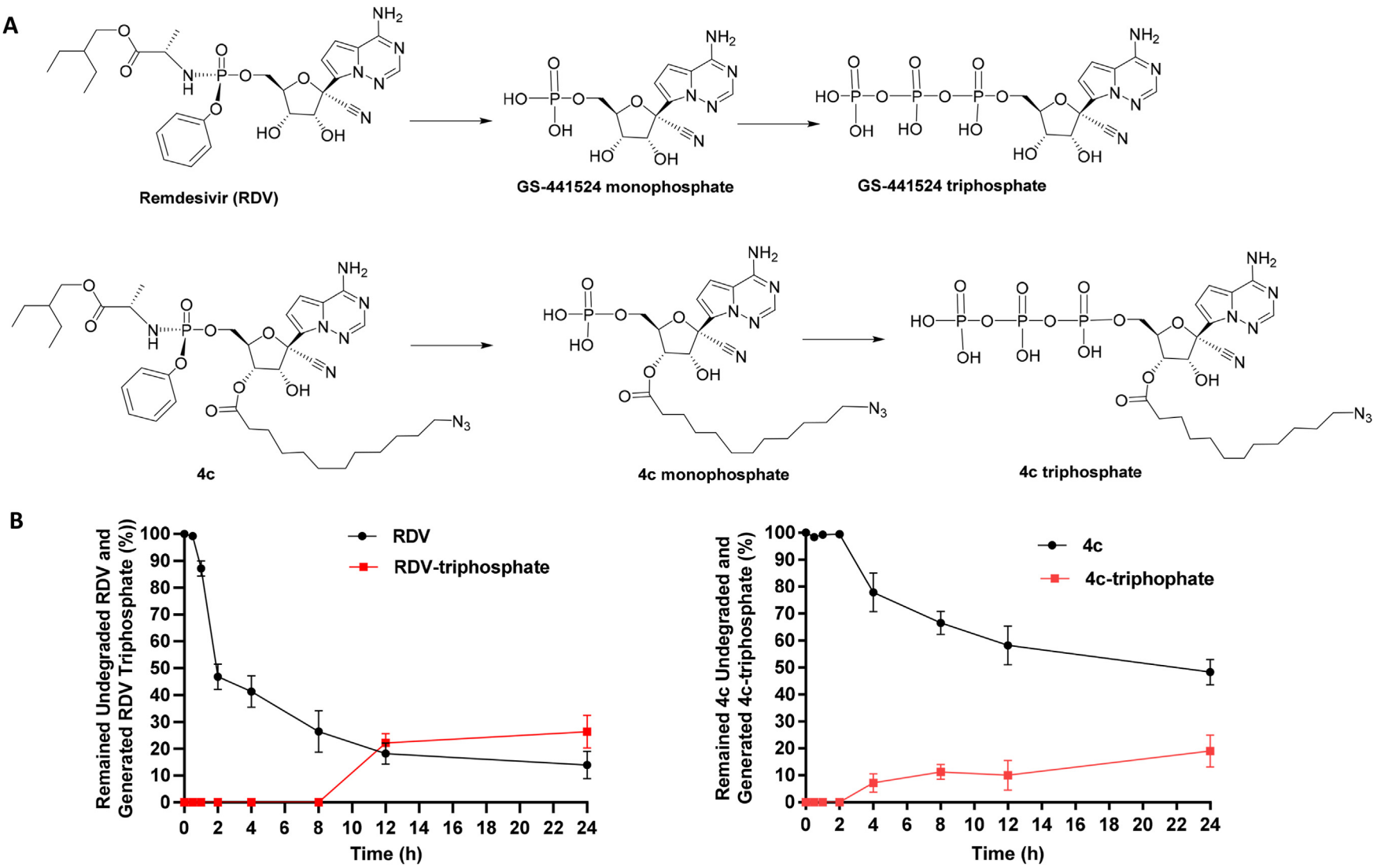

Fig. 2. A) Chemical structures of parent molecules and their observed metabolites in the presence of human plasma. B) Plasma stability of RDV and **4c**.

gradient system (water/acetonitrile) at a constant flow rate of 1 mL/min with UV detection at 254 nm. Analytical HPLC confirmed the purity of the final products. The chemical structures of final products were characterized by nuclear magnetic resonance spectrometry 1D NMR (^{1}H, ^{13}C) and 2D NMR spectra (HSQC, HSQC-TOCSY, HMBC, COSY) measured on a Bruker NMR spectrometer (400 MHz). The chemical shifts were reported in parts per millions (ppm). The compounds' molecular weight was confirmed by a high-resolution mass spectroscopy time-of-flight electrospray mass spectrometer using (Phenomenex Luna, 4 μm C18 150 × 4.6 mm HPLC Column).

Huh-7 (a generous gift from the Gordan lab at the University of California at San Fransico), Vero E6 (ATCC# CRL-1586), and Calu3 (ATCC# HTB-55) cells were maintained in Dulbecco's minimal essential medium (DMEM) with 10% fetal bovine serum (FBS) and cultured at 37 °C and 5% CO_2. SARS-CoV-2, strain USA/WA1/2020, was obtained from the World Reference Collection for Emerging Viruses and Arboviruses at the University of Texas Medical Branch-Galveston. Stocks of SARS-CoV-2 were grown and titered on Vero E6 cells as described previously [32]. pCAGGS VP35, pCAGGS NP, pCAGGS VP30, pCAGGS L, pCAGGS T7 and a constitutively expressed firefly plasmid, pCAGGS ce-FF, were previously [34,35]. The EBOV tetracistronic minigenome (EBOV trVLP) reporter was synthesized by Genscript, based on the tetracistronic minigenome described in Watt et al. [31], and cloned into the plasmid pM1.

4.2. Preparation of fatty acyl chloride

The fatty acids namely 12-azidododecanoic acid and 12-ethylthiododecanoic acid were prepared according to the previously reported methods described [36,37], and purified by HPLC. The appropriate fatty acid (3.0 mmol) was dissolved in 5 mL of anhydrous benzene. Then oxalyl chloride (300 μL, 3.6 mmol) was added to the solution of fatty acid, and the reaction mixture was stirred at room temperature (25 °C) for 5 h. The solvents were evaporated to dryness under reduced pressure to get the corresponding fatty acid chloride as yellow syrup.

4.3. General procedure for the synthesis of monofatty acyl RDV conjugates 3a-e and 4a-e

RDV (**1**, 61 mg, 0.1 mmol) was dissolved in an anhydrous DCM/THF (2:1, 40 mL) followed by addition of DIPEA (8 equiv, 140 μL, 0.8 mM). The freshly prepared acid chloride (**2a-e**, 1.5 equiv, 0.15 mmol) was dissolved in 10 mL of anhydrous DCM and added to the mixture dropwise over 60 min. The reaction mixture was kept stirring at 40 °C for 6–9 h. LC/MS was used to monitor the progress of the reaction. Upon completing the reaction, the reaction mixture was cooled down to room temperature, the solvents were evaporated to dryness, and the crude product was dissolved in acetonitrile + water + 0.1% trifluoroacetic acid (TFA). A C18 reverse phase column was used for purification and separation of different isomers of conjugates **3a-e** and **4a-e** using a gradient of acetonitrile/water containing 0.1% TFA at the flow rate of 7 mL/min using a semipreparative HPLC system.

4.3.1. (2R,3R,4R,5R)-2-(4-Aminopyrrolo[2,1-f][1,2,4]triazin-7-yl)-2-cyano-5-((((((R)-1-(2-ethylbutoxy)-1-oxopropan-2-yl) amino)(phenoxy)phosphoryl)oxy)methyl)-4-hydroxytetra-hydrofuran-3-yl tetradecanoate (3a)

Compound **3a** was obtained by the reaction of **1** with myristoyl chloride (**2a**). Yield (3.23 mg, 5.3%, colorless solid). ^{1}H NMR (400 MHz, $CDCl_3$) δ 7.81 (s, 1H), 7.30 (t, J = 7.6 Hz, 2H), 7.17 (d, J = 7.6 Hz, 3H), 7.09 (d, J = 5.6 Hz, 1H), 6.99 (d, J = 4.8 Hz, 1H), 5.82 (d, J = 5.6 Hz, 1H), 4.54–4.44 (m, 2H), 4.42–4.35 (m, 2H), 4.06 (dd, J = 6.0, 6.0 Hz, 1H), 3.98 (dd, J = 5.6, 6.0 Hz, 1H), 3.95–3.90 (m, 1H), 2.62 (br, 1H, NH), 2.52 (t, J = 7.6 Hz, 2H), 1.72–1.63 (m, 2H), 1.54–1.46 (m, 1H), 1.36–1.25 (m, 27H), 0.89–0.84 (m, 9H). ^{13}C NMR (101 MHz, $CDCl_3$) δ 173.81, 172.75, 151.22, 150.54, 136.38, 130.03, 129.87, 125.44, 120.02, 115.17, 114.62, 114.02, 109.22, 82.54, 78.36, 74.58, 69.31, 68.02, 65.05, 50.37, 40.33, 34.22, 32.07, 29.80, 29.63, 29.51, 29.37, 29.21, 24.83, 23.29, 22.84, 21.06, 14.27, 11.10, HR-MS (ESI-TOF) (m/z): $C_{41}H_{61}N_6O_9P$, calcd., 812.9458; found, 813.4431 $[M + H]^+$.

4.3.2. ((2R,3R,4R,5R)-2-(4-Aminopyrrolo[2,1-f][1,2,4]triazin-7-yl)-2-cyano-5-((((((R)-1-(2-ethylbutoxy)-1-oxopropanyl) amino)(phenoxy)phosphoryl)oxy)methyl)-4-hydroxytetra- hydrofuran-3-yl 3-(decyloxy)propanoate (3b)

Compound **3b** was obtained by the reaction of **1** with 3-(decyloxy)propanoyl chloride (**2b**). Yield (3.3 mg, 5.3%, colorless solid). ^{1}H NMR (400 MHz, $CDCl_3$) δ 7.85 (s, 1H), 7.28 (t, J = 7.6 Hz, 2H), 7.15 (dd, J = 8.4, 7.6 Hz, 3H), 7.08 (d, J = 5.6 Hz, 1H), 6.99 (d, J = 5.6 Hz, 1H), 5.83 (d, J = 5.6 Hz, 1H), 4.53–4.43 (m, 2H), 4.43–4.31 (m, 2H), 4.08 (dd, J = 5.6, 6.0 Hz, 1H), 4.00–3.95 (m, 2H), 3.94–3.88 (m, 1H), 3.73–3.65 (m, 2H), 3.55–3.42 (m, 2H), 2.76 (t, J = 7.6 Hz, 2H), 1.57–1.47 (m, 3H), 1.34–1.23 (m, 24H), 0.89–0.84 (m, 9H). ^{13}C NMR (101 MHz, $CDCl_3$) δ 173.53, 172.62, 150.65, 150.46, 137.57, 130.21, 128.03, 124.98, 120.09, 115.99, 114.68, 113.77, 107.31, 82.38, 78.37, 74.70, 71.54, 69.43, 67.99, 65.70, 65.07, 50.36, 40.31, 34.22, 32.06, 29.80 29.63, 29.50, 29.41, 29. 27, 26.13, 23.29, 22.83, 21.16, 14.27, 11.05. HR-MS (ESI-TOF) (m/z): $C_{40}H_{59}N_6O_{10}P$, 814.9178; found, 815.4182 $[M + H]^+$.

4.3.3. (2R,3R,4R,5R)-2-(4-Aminopyrrolo[2,1-f][1,2,4]triazin-7-yl)-2-cyano-5-((((((R)-1-(2-ethylbutoxy)-1-oxopropan-2-yl) amino)(phenoxy)phosphoryl)oxy)methyl)-4-hydroxytetra hydrofuran-3-yl palmitate (3c)

Compound **3c** was obtained by the reaction of **1** with 12-azidododecanoyl chloride (**2c**). Yield (4.27 mg, 7%, colorless solid). ^{1}H NMR (400 MHz, $CDCl_3$) δ 7.80 (s, 1H, H-2 of the pyrrolotriazine ring), 7.29 (t, J = 7.6 Hz, 2H), 7.18 (d, J = 8.0 Hz, 3H), 7.14 (d, J = 4.8 Hz, 1H), 6.99 (d, J = 4.4 Hz, 1H), 5.81 (d, J = 5.2 Hz, 1H), 4.53–4.43 (m, 2H), 4.43–4.33 (m, 2H), 4.14 (t, 1H) 4.06 (dd, J = 5.8, 5.8 Hz, 1H), 3.99 (dd, J = 5.7, 5.6 Hz, 2H), 3.25 (t, J = 6.8 Hz, 2H), 2.52 (t, J = 7.6 Hz, 2H), 1.72–1.65 (m, 2H), 1.62–1.55 (m, 2H), 1.52–1.46 (m, 1H), 1.36–1.27 (m, 23 Hs), 0.86 (t, J = 7.4 Hz, 6H). ^{13}C NMR (101 MHz, $CDCl_3$) δ 173.82, 172.49, 150.98, 150.53, 137.39, 130.03 128.13, 125.44, 119.96, 114.58, 114.31, 114.01, 108.10, 82.54, 78.34, 74.61, 69.20, 68.02, 64.92, 51.63, 50.40, 40.33, 34.19, 29.58, 29.26, 29.16, 28.96, 26.84, 24.80, 23.29, 21.02, 11.10. HR-MS (ESI-TOF) (m/z): $C_{39}H_{56}N_9O_9P$, calcd, 825.9048; found, 826.4096 $[M + H]^+$.

4.3.4. (2R,3R,4R,5R)-2-(4-Aminopyrrolo[2,1-f][1,2,4]triazin-7-yl)-2-cyano-5-((((((R)-1-(2-ethylbutoxy)-1-oxopropan-2-yl) amino)(phenoxy)phosphoryl)oxy)methyl)-4-hydroxytetra hydrofuran-3-yl palmitate (3d)

Compound **3d** was obtained by the reaction of **1** with palmitoyl chloride (**2d**). Yield (6.0 mg, 10%, colorless solid). ^{1}H NMR (400 MHz, $CDCl_3$) δ 7.82 (s, 1H), 7.30 (t, J = 7.6 Hz, 2H), 7.18 (dd, J = 8.0, 8.0 Hz, 3H), 7.11 (d, J = 4.4 Hz, 1H), 6.98 (d, J = 4.8 Hz, 1H), 5.82 (d, J = 5.6 Hz, 1H), 4.52–4.45 (m, 2H), 4.40–4.30 (m, 2H), 4.07 (dd, J = 6.0, 6.0 Hz, 1H), 4.00 (dd, J = 5.6, 5.6 Hz, 1H), 3.93–3.86 (m, 1H), 2.50 (t, J = 7.6 Hz, 2H), 1.71–1.59 (m, 2H), 1.53–1.47 (m, 1H), 1.37–1.25 (m, 31H), 0.89–0.84 (m, 9H). ^{13}C NMR (101 MHz, $CDCl_3$) δ 173.46, 172.52, 150.80, 150.46, 137.22, 130.05, 128.43, 125.45, 120.05, 115.20, 114.57, 114.11, 108.11, 82.50, 78.33, 74.65, 69.30, 68.02, 65.00, 50.42, 40.33, 34.22, 32.07, 29.85, 29.64, 29.51, 29.36, 29.23, 24.84, 23.26, 22.84, 21.08, 14.27, 11.06. HR-MS (ESI-TOF) (m/z): $C_{43}H_{65}N_6O_9P$, 840.9866; found, 841.4703 $[M + H]^+$.

4.3.5. 2R,3R,4R,5R)-2-(4-Aminopyrrolo[2,1-f][1,2,4]triazin-7-yl)-2-cyano-5-((((((®-1-(2-ethyl-butoxy)-1-oxopropanyl) amino)(phenoxy)phosphoryl)oxy)methyl)-4-hydroxy-tetrahydrofuran-3-yl 12-(ethylthio)dodecanoate (3e)

Compound **3e** was obtained by the reaction of **1** with 12-(ethylthio)dodecanoyl chloride (**2e**). Yield (5.49 mg, 9%, colorless solid). ^{1}H NMR (400 MHz, $CDCl_3$) δ 7.79 (s, 1H), 7.30 (t, J = 7.6 Hz, 2H), 7.19 (dd, J = 7.2, 8.4 Hz, 3H), 7.11 (d, J = 4.8 Hz, 1H), 6.93 (d, J = 4.8 Hz, 1H), 5.84 (d, J = 5.6 Hz, 1H), 4.51–4.44 (m, 2H), 4.39–4.30 (m, 2H), 4.18 (t, 1H), 4.06 (dd, J = 6.0, 6.0 Hz, 1H), 3.97 (dd, J = 5.6, 6.0 Hz, 1H), 3.94–3.89 (m, 1H), 2.56–2.45 (m, 6H), 1.72–1.65 (m, 2H), 1.61–1.53 (m, 2H), 1.51–1.46 (m, 1H), 1.36–1.23 (m, 24H), 0.88–0.83 (dt, J = 4.36, 7.4 Hz, 6H). ^{13}C NMR (101 MHz, $CDCl_3$): δ 173.49, 172.58, 151.51, 150.50, 138.65, 130.00, 127.30, 125.38, 120.06, 115.44, 114.76, 116.66, 107.36, 82.53, 78.47, 74.58, 69.27, 67.96, 65.72, 50.36, 40.18, 34.11, 31.80, 29.78, 29.64, 29.58, 29.37, 29.17, 29.09, 26.05, 24.83, 23.28, 21.10, 14.96, 11.04. HR-MS (ESI-TOF) (m/z): $C_{41}H_{61}N_6O_9PS$ 844.9995; found, 845.4168 $[M + H]^+$.

4.3.6. (2R,3S,4R,5R)-5-(4-Aminopyrrolo[2,1-f][1,2,4]triazin-7-yl)-5-cyano-2-((((((R)-1-(2-ethylbutoxy)-1-oxopropan-2-yl) amino)(phenoxy)phosphoryl)oxy)methyl)-4-hydroxy tetrahydrofuran-3-yl tetradecanoate (4a)

Compound **4a** was obtained by the reaction of **1** with myristoyl chloride (**2a**). Yield (39.6 mg, 65%, colorless solid). ^{1}H NMR (400 MHz, $CDCl_3$) δ 7.85 (s, 1H), 7.19 (t, J = 7.6 Hz), 7.07 (dd, J = 5.6, 3.2 Hz, 3H), 7.01 (d, J = 5.2 Hz, 1H), 6.92 (d, J = 4.4 Hz, 1H), 5.33 (dd, J = 2.8, 2.8 Hz, 1H), 4.71 (d, J = 6 Hz, 1H), 4.60–4.54 (br. m, 1H), 4.41–4.30 (m, 2H), 4.07 (dd, J = 5.6 Hz, 5.6 Hz, 1H), 3.99–3.94 (m, 2H), 3.93–3.88 (m, 1H), 2.48 (dt, J = 7.6 Hz, 2.8 Hz, 2H), 1.73–1.65 (m, 2H), 1.53–1.47 (m, 1H), 1.35–1.25 (m, 27H), 0.89–0.85 (m, 9H). ^{13}C NMR (101 MHz, $CDCl_3$) δ 173.64, 173.54, 152.83, 150.46, 141.79, 130.01, 129.81, 125.23, 120.08, 115.58, 114.88, 112.92 105.55, 83.28, 78.67, 75.04, 72.39, 67.93, 65.77, 50.37, 40.31, 34.19, 32.06, 29.80, 29.63, 29.50, 29.40, 29.26, 24.85, 23.25, 22.83, 21.12, 14.27, 11.10. HR-MS (ESI-TOF) (m/z): $C_{41}H_{61}N_6O_9P$ calcd., 812.4635 found, 813.4425 $[M + H]^+$.

4.3.7. (2R,3S,4R,5R)-5-(4-Aminopyrrolo[2,1-f][1,2,4]triazin-7-yl)-5-cyano-2-((((((R)-1-(2-ethylbutoxy)-1-oxopropan-2-yl) amino)(phenoxy)phosphoryl)oxy)methyl)-4-hydroxy-tetrahydrofuran-3-yl-3-(decyloxy)propanoate (4b)

Compound **4b** was obtained by the reaction of **1** with 3-(decyloxy)propanoyl chloride (**2b**). Yield (32.3 mg, 53%, colorless solid). ^{1}H NMR (400 MHz, $CDCl_3$) δ 7.86 (s, 1H), 7.24 (t, J = 7.6 Hz, 2H), 7.09 (t, J = 8 Hz, 3H), 7.04 (d, J = 3.2 Hz, 1H), 6.98 (d, J = 4.0 Hz, 1H), 5.53 (dd, J = 2.0, 2.4 Hz, 1H), 4.84 (d, J = 5.6 Hz, 1H), 4.64–4.57 (br. m, 1H), 4.40–4.30 (m, 2H), 4.08 (dd, J = 6.0, 6.0 Hz, 1H), 3.99 (dd, J = 6.0, 5.6 Hz, 1H), 3.96–3.90 (m, 2H), 3.80–3.66 (m, 2H), 3.55–3.42 (m, 2H), 2.77 (t, J = 6.0 Hz, 2H), 1.55–1.46 (m, 3H), 1.35–1.25 (m, 21H), 0.90–0.85 (m, 9H). ^{13}C NMR (101 MHz, $CDCl_3$) δ 173.48, 170.42, 151.72, 150.45, 138.99, 129.91, 127.63, 125.36, 120.15, 115.37, 114.01, 113.86, 107.01, 82.83, 78.27, 75.41, 72.01, 71.72, 67.95, 65.86, 65.69, 50.39, 40.33, 35.43, 32.03, 29.72, 29.55, 29.45, 26.06, 23.26, 22.82, 21.20, 14.26, 11.06. HR-MS (ESI-TOF) (m/z): $C_{40}H_{59}N_6O_{10}P$ 814.9178; found, 815.4215 $[M + H]^+$.

4.3.8. (2R,3S,4R,5R)-5-(4-Aminopyrrolo[2,1-f][1,2,4]triazin-7-yl)-5-cyano-2-((((((R)-1-(2-ethylbutoxy)-1-oxopropan-2-yl) amino)(phenoxy)phosphoryl)oxy)methyl)-4-hydroxy-tetrahydrofuran-3-yl-12-azidododecanoate (4c)

Compound **4c** was obtained by the reaction of **1** with 12-azidododecanoyl chloride (**2c**). Yield (30.50 mg, 50%, colorless solid). ^{1}H NMR (400 MHz, $CDCl_3$) δ 7.84 (s, 1H), 7.22 (t, J = 7.2 Hz, 2H), 7.18 (d, J = 7.6 Hz, 1H), 7.06 (dd, J = 6.8, 7.6 Hz, 3H), 6.98 (d, J = 3.6 Hz, 1H), 5.30 (dt, J = 2.8, 3.2 Hz, 1H), 4.77 (d, J = 5.2 Hz, 1H), 4.62–4.54 (br. m, J = 5.6 Hz, 1H), 4.44–4.29 (m, 2H), 4.06 (dd, J = 6.0, 6.0 Hz, 1H), 3.99 (dd, J = 5.6, 5.6 Hz, 1H), 3.93–3.85 (m, 1H), 3.81 (d, J = 7.6 Hz, 1H), 3.25 (t, J = 6.8 Hz, 2H), 2.48 (t, J = 7.6 Hz, 2H), 1.71–1.66 (m, 2H), 1.61–1.55 (m, 2H), 1.52–1.46 (m, 1H), 1.35–1.25 (m, 23H), 0.87 (t, J = 7.6 Hz, 6H). ^{13}C NMR (101 MHz, $CDCl_3$) δ 173.63, 173.51, 150.83, 150.31, 137.73, 129.94, 128.40, 125.42, 120.06, 115.28, 114.15, 113.90, 108.62, 83.23, 78.35, 74.93, 72.23, 67.99, 65.81, 51.62, 50.37, 40.31, 34.16, 29.84, 29.57, 29.33, 29.27, 28.96, 26.84, 24.82, 23.24, 20.99, 11.10. HR-MS (ESI-TOF) (m/z): $C_{39}H_{56}N_9O_9P$: 825.9048, 826.4135 $[M + H]^+$.

4.3.9. (2R,3S,4R,5R)-5-(4-Aminopyrrolo[2,1-f][1,2,4]triazin-7-yl)-5-cyano-2-((((((R)-1-(2-ethylbutoxy)-1-oxopropan-2-yl) amino)(phenoxy)phosphoryl)oxy)methyl)-4-hydrox-ytetrahydrofuran-3-yl pentadecanoate (4d)

Compound **4d** was obtained by the reaction of **1** with palmitoyl chloride (**2d**). Yield (39.0 mg, 64%, colorless solid). ^{1}H NMR (400 MHz, $CDCl_3$) δ 7.86 (s, 1H, H-2 of the pyrrolotriazine ring), 7.22 (t, J = 7.6 Hz, 2H), 7.18 (d, J = 7.6 Hz, 1H),7.09 (dd, J = 7.2, 8.0 Hz, 3H), 6.98 (d, J = 4.8 Hz, 1H), 5.30 (dd, 1H, J = 2.4, 2.8 Hz), 4.76 (d, J = 6.0 Hz, 1H), 4.60–4.53 (br. m, 1H), 4.45–4.29 (m, 2H), 4.06 (dd, J = 5.6, 6.0 Hz,1H), 3.99 (dd, J = 5.6, 6.0 Hz, 1H), 3.93–3.85 (m, 1H), 2.46 (t, J = 7.6 Hz, 2H), 1.72–1.62 (m, 2H), 1.53–1.47 (m, 1H), 1.33–1.25 (m, 31H), 0.89–0.85 (m, 9H). ^{13}C NMR (101 MHz, $CDCl_3$) δ 173.51, 173.43, 150.37, 150.27, 136.44, 129.95, 129.13, 125.52, 120.04, 114.99, 114.22, 113.79, 109.26, 83.29, 78.22, 75.10, 72.13, 68.04, 65.87, 50.35, 40.31, 34.15, 32.07, 29.81, 29.63, 29.51, 29.39, 29.25, 24.84, 23.23, 22.84 (CH2-15 of the fatty acid moiety), 20.89, 14.27, 11.02. HR-MS (ESI-TOF) (m/z): $C_{43}H_{65}N_6O_9P$, 840.9998; found, 841.4892 $[M + H]^+$.

4.3.10. ((2R,3S,4R,5R)-5-(4-Aminopyrrolo[2,1-f][1,2,4]triazin-7-yl)-5-cyano-2-((((((R)-1-(2-ethyl-butoxy)-1-oxopropan-2-yl) amino)(phenoxy)phosphoryl)oxy)methyl)-4-hydroxy-tetrahydrofuran-3-yl 12-(ethylthio)dodecanoate (4e)

Compound **4e** was obtained by the reaction of **1** with 12-(ethylthio)dodecanoyl chloride (**2e**). Yield (33.6 mg, 55%, colorless solid). ^{1}H NMR (400 MHz, $CDCl_3$) δ 7.83 (s, 1H), 7.23 (t, J = 7.6 Hz, 2H), 7.17 (d, J = 7.2 Hz, 1H), 7.08 (dd, J = 7.6, 7.2 Hz, 3H), 6.96 (d, J = 4.0 Hz, 1H), 5.31 (dd, J = 2.8, 2.8 Hz, 1H), 4.81 (d, J = 5.2 Hz, 1H), 4.61–4.53 (m, J = 6.0 Hz, 1H), 4.41–4.34 (m, 2H), 4.06 (dd, J = 5.6, 5.6 Hz, 1H), 3.98 (dd, J = 6.0, 5.6 Hz, 1H), 3.94–3.90 (m, 1H), 2.52–2.43 (m, 6H), 1.72–1.63 (m, 2H), 1.61–1.53 (m, 2H), 1.52–1.47 (m, 1H), 1.34–1.23 (m, 24H), 0.87 (t, J = 7.6 Hz, 6H). ^{13}C NMR (101 MHz, $CDCl_3$), δ 173.85, 173.48, 150.71, 150.38, 137.96, 129.93, 128.42, 125.41, 120.07, 115.23, 114.17, 113.83, 108.41, 83.24, 78.34, 75.07, 72.23, 67.99, 65.82, 50.39, 40.32, 34.17, 33.74, 32.96, 31.80, 29.80, 29.65, 29.57, 29.36, 29.24, 29.11, 28.89, 28.30, 26.04, 24.83, 23.25, 21.09, 14.98, 11.10. HR-MS (ESI-TOF) (m/z): $C_{41}H_{61}N_6O_9PS$ 844.9995; found, 845.4116 $[M + H]^+$.

4.4. General procedure for the synthesis of difatty acyl remdesivir conjugates 5a-b

A solution of **1** (20.40 mg, 0.033 mmol) was dissolved in an anhydrous DCM/THF (2:1, 20 mL) containing DIPEA (~8 equiv, 47 μL, 0.27 mM). Then this solution was added gradually on three portions to a solution of freshly prepared fatty acyl chloride (5 equiv, 0.165 mmol) dissolved in 10 mL of anhydrous DCM. The reaction mixture was kept stirring at 40 °C for 6–9 h. LC/MS was used to monitor the progress of the reaction. Upon completing the reaction, the reaction mixture was cooled down to room temperature, the solvents were evaporated to dryness, and the crude product was dissolved in acetonitrile + water +0.1% TFA. The crude compound

was purified using a C18 column as mentioned above.

4.4.1. ((2R,3R,4R,5R)-2-(4-Aminopyrrolo[2,1-f][1,2,4]triazin-7-yl)-2-cyano-5-((((((R)-1-(2-ethylbutoxy)-1-oxopropan-2-yl)amino)(phenoxy)phosphoryl)oxy)methyl)tetrahydro-furan-3,4-diyl ditetradecanoate (5a)

Compound **5a** was obtained by the reaction of **1** with myristoyl chloride (**2a**). Yield (~17.4 mg, 85.0%, colorless solid). ^{1}H NMR (400 MHz, $CDCl_3$) δ 7.94 (s, 1H), 7.29 (t, J = 7.6, 2H), 7.15 (dd, J = 8.4, 7.2 Hz, 3H), 6.85 (d, J = 4.4, 1H), 6.57 (d, J = 4.8 Hz, 1H), 6.22 (d, J = 5.6 Hz, 1H), 6.15–5.90 (br s, 2H), 5.52 (dt, J = 4.8, 0.8 Hz), 4.58 (dd, J = 4.0, 4.0 Hz 1H), 4.39 (dd, J = 5.6, 4.4 Hz, 2H), 4.06 (dd, J = 5.6, 6.0 Hz, 1H), 4.01 (d, J = 3.2 Hz, 1H), 3.99 (dd, J = 6.0, 6.0 Hz, 2H), 2.42–2.35 (m, 4H), 1.52–1.45 (m, 1H), 1.36–1.24 (m, 47H), 0.89–0.84 (m, 12 Hs). ^{13}C NMR (101 MHz, $CDCl_3$) δ 173.58, 172.71, 171.87, 150.69, 150.62, 146.95, 129.85, 125.12, 122.11, 120.23, 117.02, 115.32, 112.78, 100.77, 82.07, 71.99, 70.45, 67.75, 65.45, 50.36, 40.31, 34.01, 32.06, 29.80, 29.77, 29.63, 29.50, 29.45, 29,39, 29.20, 24.86, 24.75 23.29, 22.72, 21.25, 14.26, 11.06. HR-MS (ESI-TOF) (m/z): $C_{55}H_{87}N_6O_{10}P$, calcd., 1023.3068; found, 1023.6637 $[M]^+$.

4.4.2. (2R,3R,4R,5R)-2-(4-Aminopyrrolo[2,1-f][1,2,4]triazin-7-yl)-2-cyano-5-((((((R)-1-(2-ethylbutoxy)-1-oxopropan-2-yl)amino)(phenoxy)phosphoryl)oxy)methyl)tetrahydrofuran-3,4-diyl ditetradecanoate (5b)

Compound **5b** was obtained by the reaction of **1** with 12-azidododecanoyl chloride (**2c**). Yield (15.3 mg, 75%, colorless solid). ^{1}H NMR (400 MHz, $CDCl_3$) δ 7.76 (s, 1H), 7.28 (t, J = 8.0 Hz, 2H), 7.14 (t, J = 2.8, 5.6 Hz, 3H), 7.07 (d, J = 4.8 Hz, 1H), 6.90 (d, J = 4.8 Hz, 1H), 6.01 (d, J = 6.4 Hz, 1H), 5.46 (dt, J = 4.4, 1.6 Hz, 1H), 4.65–4.56 (m, 1H), 4.42–4.38 (m, 2H), 4.09 (dd, J = 6.0, 6.0 Hz, 1H), 4.05–3.95 (m, 2H), 3.81 (d, J = 3.2 Hz, 1H), 3.25 (dt, J = 6.8, 2.4 Hz, 4H), 2.42–2.35 (m, 4H), 1.69–1.55 (m, 8H), 1.53–1.47 (m, 1H), 1.39–1.25 (m, 39H), 0.88 (t, J = 7.6 Hz, 6H). ^{13}C NMR (101 MHz, $CDCl_3$) δ 173.47, 172.71, 171.73, 150.85, 150.37, 137.26, 130.01, 126.89, 125.44, 120.19, 114.63 114.51, 114.29, 107.99, 82.66, 78.91, 72.62, 70.06, 67.92, 65.41, 51.61, 50.42, 40.33, 34.03, 33.92, 32.06, 29.79, 29.60, 29.40, 29.28, 29.18, 28.97, 28.79, 26.85 & 24.84, 24.70, 23.30, 22.84, 11.10. HR-MS (ESI-TOF) (m/z): $C_{51}H_{77}N_{12}O_{10}P$, 1049.2077; found, 1049.6035 $[M]^+$.

4.5. General method for preparation of physical mixture 6a-d

A solution of RDV (1, 20.40 mg, 0.033 mmol) was dissolved in an anhydrous THF (5 mL) containing DIPEA (~8 equiv, 47 μL, 0.27 mM). Then an equimolar solution of the fatty acid (0.033 mmol) was prepared by dissolving the proper fatty acid (**2a-d**) in a few mL of DCM and mixed under stirring at room temperature with RDV solution. The stirring was continued for 15–20 min and then the solvents were evaporated to complete dryness. The resulted colorless solid powder was kept under vacuum for few hours to make sure the complete removal of any solvents and moisture.

4.6. Plasma stability study

The metabolic stability of RDV and one of the lead fatty acyl derivatives (**4c**) were assessed in human plasma supplemented with K_2 EDTA as an anticoagulant. For accurate quantification, we employed a high resolution mass spectrometer (LC-QTOF-MS). To remove the background interference, the data was processed by using narrower (±0.1 m/z) extracted ion chromatogram (EIC) window. Test compound (10 μM) was incubated in human plasma at 37 °C. 10 μL aliquots were taken at different time points (0, 0.5, 1, 2, 4, 8, 12, and 24 h), and the plasma proteins were precipitated by the addition of cold ethanol (200 μL) and incubated for 30 min at −20 °C. The samples were centrifuged at 9000 g for 15 min, and the supernatant was transferred to a new tube and concentrated under vacuum. The samples dissolved in water and analyzed on Kinetex (phenomenex) C18 column (100 Å, 1.7 μ, 2.10 × 50 mm) at a flow rate of 0.3 mL/min using a linear gradient of aqueous acetonitrile in the presence of formic acid (TFA; 0.1%, v/v) as ion pair reagent. The analytes were quantified by their peak areas of EIC. The percentage digestion of the test compound was calculated relative to the peak areas at 0 min.

4.7. Impedance-based Vero E6 anti-SARS-CoV-2 compound screening

Compounds were screened for anti-SARS-CoV-2 activity on Vero E6 cells using the Maestro Z real-time cellular impedance platform (Axion Biosystems, Atlanta, GA) as described previously [30]. The Maestro Z instrument monitors resistance across cell monolayers, similar to *trans*-epithelial electrical resistance (TEER) [38]. Vero E6 cells were plated to confluency (7.5×10^4 cells/well) in fibronectin-coated 96-well CytoView-Z electrode plates and docked into the Maestro Z instrument for 24-h at 37 °C and 5% CO_2 to allow resistance measurements across the cell monolayer to stabilize. For compound treatment, growth media was removed from the wells of the CytoView-Z plates, and cells were pre-treated with serial 6-fold dilutions of the indicated compound in DMEM with 2% FBS and incubated at 37 °C and 5% CO_2 for 1h. Cells were then infected with SARS-CoV-2 at an MOI of 0.01. Plates were docked into the Maestro-Z instrument, and resistance measurements were continuously recorded for 48 h. All plates contained media only and full lysis controls, as well as uninfected and SARS-CoV-2 infected DMSO-treated controls. For calculation of percent inhibition, raw resistance values were normalized to values at 1-h post-infection within the Axis-Z software. Percent inhibition was calculated with the following formula: % inhibition = 100*(1-(1-average of treated cells)/(1-average of infected control)). Fifty percent inhibitory concentration (IC_{50}) values were calculated with Prism 9 (GraphPad) using a four-parameter, nonlinear regression analysis. Compound toxicity was determined by monitoring changes in monolayer resistance between 1- and 24-h post-infection, before virus-induced cytopathic effects become apparent.

4.8. Calu3 compound testing and cytotoxicity

Calu3 cells were seeded to confluency (7.5×10^4) in 96-well plates 24-h prior to infection. The day of infection, cells were pre-treated with 3-fold dilutions of the indicated compound in DMEM with 2% FBS for 1-h followed by infection with SARS-CoV-2 at an MOI of 0.01 for 48 h. The infection was performed in the presence of the compounds. After infection, supernatants were harvested and stored at −80 °C until further analysis. To determine half-maximal cell cytotoxicity concentration (CC_{50}) values of the tested compounds, Calu3 cells (1×10^4) were plated in black clear-bottom 96-well plates and 24 h later 3-fold serial dilutions of compounds were added. Forty-eight hours post-treatment, CellTox green (Promega) was added, and fluorescent dye incorporation was determined using an EnVision plate reader. CC_{50} values were calculated with Prism 9 (GraphPad) using a four-parameter, nonlinear regression analysis.

4.9. Quantification of SARS-CoV-2 from Calu3 compound testing

Supernatants from infected cultures were harvested and titered by immunofocus-forming assay on Vero E6 cells as previously described [32,33] of serially diluted supernatants from infected, compound treated Calu3 cells were plated onto confluent Vero E6

cells in 96-well plates for 1 h. After 1 h of adsorption at 37 °C and 5% CO_2, 40 μL of 2.4% microcrystalline cellulose (MCC) overlay was added to each well of the 96-well plate to achieve a final MCC overlay concentration of 1.2%. Plates were then incubated at 37 °C and 5% CO_2 for 24-h. The MCC overlay was gently removed and cells were fixed with 10% neutral buffered formalin (NBF) for 1 h at room-temperature (RT). After removal of NBF, monolayers were washed with ultrapure water and ice-cold 100% methanol with 0.3% H_2O_2 was added for 30 min to permeabilize the cells and quench endogenous peroxidase activity. Monolayers were then blocked in 5% non-fat dry milk (NFDM) in PBS for 1 h and subsequently incubated with SARS-CoV N primary antibody (Novus Biologicals; NB100-56576−1:2000) overnight at 4 °C in PBS, 5% NFDM. Monolayers were washed with PBS and incubated with an HRP-conjugated secondary antibody (Cell Signaling; 7074) for 1 h at RT in PBS, 5% NFDM. The secondary antibody was removed, monolayers were washed with PBS, and the assay was developed using TrueBlue substrate (KPL) for 30 min. Plates were imaged, and foci were counted by eye and recorded as focus forming units per milliliter (ffu/mL). Half-maximal inhibitory concentration (IC_{50}) values were calculated with Prism 9 (GraphPad) using a four-parameter, nonlinear regression analysis.

4.10. Ebola trVLP assay

To generate EBOV transcription and replication competent virus like particles (trVLPs), Huh-7 cells (1×10^7) were plated in a 150 mm dish for 24 h. Cells were then transfected using TransIT-LT1 (Mirius Bio) (ratio of 3 μl LT1 to 1 μg DNA) with the following plasmid amounts: 1.25 μg pCAGGS VP35, 1.25 μg pCAGGS NP, 0.75 μg pCAGGS VP30, 10 μg pCAGGS L, 2.5 μg pCAGGS T7 and 2.5 μg pM1 EBOV trVLP in 25 mL of 10% FBS DMEM. Seventy-two hours post transfection, the supernatant was collected and the trVLPs were precipitated using 5x PEG virus precipitation kit (BioVision). The pellet was resuspended in 2.5 mL of 10% FBS DMEM, aliquoted, flash frozen and stored at −80 °C.

To test the compound activity against the EBOV trVLP, Huh-7 cells (3×10^4) were transfected in suspension in 96-well format with TransIT-LT1 (ratio of 3 μl LT1 to 1 μg DNA) using a master mix, such that each well received 20 ng pCAGGS VP35, 20 ng pCAGGS NP, 12.5 ng pCAGGS VP30, 166 ng pCAGGS L and 2.5 ng of (pCAGGS ce-FF). Twenty-four hours post transfection, compounds were added in triplicate (0−50 μM, 2-fold dilution series) for 1 h after which wells were infected with a volume of trVLP resulting in $5–10 \times 10^6$ relative luciferase units (RLU) at 24-h post infection. This volume was determined by titering the trVLP stock on Huh-7 cells transfected as above in 96-well plate format (0−50 μl of trVLP, 2-fold dilution series). Twenty-four hours post infection, luciferase activity was read using a dual luciferase assay (Promega) and an EnVision plate reader. Half-maximal inhibitory concentration (IC_{50}) values were calculated with Prism 9 (GraphPad) using a four-parameter, nonlinear regression analysis.

To determine half-maximal cell cytotoxicity concentration (CC_{50}) values, Huh-7 cells (1×10^3) were plated in a 96-well plate, and 24-h later compounds were added in triplicate (0−50 μM, 2-fold dilution series). Twenty-four hours post-treatment, CellTiter-Glo (Promega) was added, and ATP content was determined by reading the luminescence using an EnVision plate reader. CC_{50} values were calculated with Prism 9 (GraphPad) using a four-parameter, nonlinear regression analysis.

4.11. Quantificaiton of SARS-CoV-2 and EBOV trVLP RNA synthesis

SARS-CoV-2 or EBOV trVLP infection with drug treatment (RDV (1 μM), **3a** (5 μM), **4b** (5 μM), **5a/5b** (45 μM)) were performed as previously described. RNA was extracted from cell monolayers using TRIzol reagent (ThermoFisher). Post extraction, RNA was DNase treated using ezDNase (ThermoFisher, Waltham, MA, USA) and subjected to first strand synthesis using SuperScript IV (ThermoFisher, Waltham, MA, USA) using the included random hexamer primers. qPCR was performed using PerfeCTa SYBR Green FastMix (VWR, Radnor, PA, USA) and primers for SARS-CoV-2 N (FWD: TAATCAGACAAGGAACTGATTA, REV: CGAAGGTGTGACTTCCATG) or Renilla luciferase (Fwd: AACGCGGCCTCTTCTTATTT, Rev: ATTTGCCTGATTTGCCCATA) and EBOV glucoprotein (GP) (Fwd: CAGCAGCGCCAGACGGGATT, Rev: GCAAAGTCTCCGGCACACGGT). RPS11 (FWD: GCCGAGACTATCTGCACTAC, REV: ATGTCCAGCCTCA-GAACTTC) was used as an internal control [39,40]. Each assay was performed in triplicate with two technical replicates, and each assay contained no-template controls. Data were analyzed by the ΔΔCt method with RPS11 serving as the housekeeping gene and uninfected DMSO treated cells as a mock control.

4.12. EBOV assay

HeLa cells were plated (4×10^3) in a 384-well plate and grown overnight. The next day, cells were treated with compounds (starting at 5 mM with 2-fold serial dilutions) in duplicate to yield a 10-point dose curve. Each well was infected in a BSL-4 laboratory at the National Emerging Infectious Diseases Laboratories (NEIDL) with wild type EBOV at a MOI of 0.3. Cells were incubated with virus for 24 h at which point they were fixed by immersion into formalin overnight at 4 °C. The formalin was removed and plates were washed three times with PBS. Cells were stained with EBOV GP specific antibody 4F3 (IBT Bioservices, MD, USA) followed by Alexa546 secondary antibody. Cell nuclei were stained using Hoechst at 1:50 000, and plates were imaged using a Cytation 1 (Biotek, VT, USA) automated microscope and nuclei and infected cells were counted using Cell Profiler software (Broad Inst. MA, USA). Infection efficiency was calculated as the ratio of infected to cell nuclei and normalized to vehicle (0.2% DMSO) treated controls.

5. Statistical analysis

IC_{50} and CC_{50} values were determined by fitting normalized percent inhibition data with a four parameter, non-linear regression in Graphpad Prism 9.

Supplementary materials

Supplementary data to this article can be found online to report NMR and Mass Spectroscopy spectra of synthesized compounds as well as antiviral data for SARS-CoV-2 and EBOV trVLP and live EBOV experiments.

Author contributions

Naglaa Salem El-Sayed: performed the chemistry, wrote the manuscript, contributed equally to this work. **Alexander S. Jureka**: conducted the antiviral and cytotoxicity assays, wrote the manuscript, contributed equally to this work. **Megan R. Edwards**: conducted the antiviral and cytotoxicity assays, wrote the manuscript, contributed equally to this work. **Sandeep Lohan**: conducted stability assays and wrote the manuscript. **Caroline G. Williams**: conducted the antiviral and cytotoxicity assays. **Patrick T. Keise**: conducted the antiviral and cytotoxicity assays. **Robert A. Davey**: conducted the antiviral and cytotoxicity assays. **Jennifer Totonchy**: conducted the antiviral and cytotoxicity assays. **Rakesh K. Tiwari**: planned and designed the experiments, contributed reagents/materials/analysis tools, wrote the manuscript. **Christopher F. Basler**:

planned and designed the experiments, contributed reagents/materials/analysis tools, wrote the manuscript. **Keykavous Parang**: planned and designed the experiments, contributed reagents/materials/analysis tools, wrote the manuscript. All authors have read and agreed to the published version of the manuscript.

Funding

This project was supported from funds from Dr. Assad Kazeminy, AJK Biopharmaceutical and Chapman University (RKT and KP) and from NIH grants AI125453 and P01AI120943 (Amarasinghe) to (CFB and RAD).

Declaration of competing interest

The increasing prevalence of COVID-19 is a severe public health problem affecting people globally. COVID-19 is taking a devastating toll on human lives. Several existing drugs and potential drug candidates such as remdesivir (RDV) have been considered for repurposing as COVID-19 treatments. Our group has previously studied the impact of fatty acylation on the antiviral activity of different anti-HIV (human immunodeficiency virus) nucleoside drugs. The conjugates were more potent and less toxic than their parent nucleoside analogs, providing a much higher selectivity index. Furthermore, the conjugates significantly enhanced the cellular uptake versus the parent analogs and corresponding physical mixtures of fatty acids and nucleosides. Herein, we report the synthesis of fatty acyl derivatives of RDV and structural characterization of their antiviral activity against SARS-CoV-2 in VeroE6 cells and Calu3 cells. Five fatty acids, myristic acid, 12-azidododecanoic acid, 12-thioethyldodecanoic acid, 4-oxatetradecanoic acid, and palmitic acid were conjugated to RDV at its 2′-*O*- and 3′-*O*-position. Most monofatty acyl derivatives of RDV demonstrated IC_{50} values against SARS-CoV-2 that were only slightly decreased relative to RDV. Against the EBOV trVLP and infectious EBOV, any of the monofatty acyl conjugates had IC_{50}s similar to that of RDV. Overall, these data together indicate that RDV can be modified with fatty acids at positions 2′ or 3′, without demonstrating a significant loss of antiviral activity in cell culture against SARS-CoV-2 and EBOV. Future studies will determine if these modifications result in greater long-acting effect, bioavailability, and stability in animal models.

Acknowledgements

The authors also acknowledge the core facility at Chapman University School of Pharmacy for providing access to the research equipment.

Appendix A. Supplementary data

Supplementary data to this article can be found online at https://doi.org/10.1016/j.ejmech.2021.113862.

References

[1] https://Coronavirus.Jhu.Edu/Map.Html.
[2] D. Siegel, H.C. Hui, E. Doerffler, M.O. Clarke, K. Chun, L. Zhang, S. Neville, E. Carra, W. Lew, B. Ross, Q. Wang, L. Wolfe, R. Jordan, V. Soloveva, J. Knox, J. Perry, M. Perron, K.M. Stray, O. Barauskas, J.Y. Feng, Y. Xu, G. Lee, A.L. Rheingold, A.S. Ray, R. Bannister, R. Strickley, S. Swaminathan, W.A. Lee, S. Bavari, T. Cihlar, M.K. Lo, T.K. Warren, R.L. Mackman, Discovery and synthesis of a phosphoramidate prodrug of a pyrrolo[2,1-f][triazin-4-amino] adenine C-nucleoside (GS-5734) for the treatment of Ebola and emerging Viruses, J. Med. Chem. 60 (2017) 1648–1661, https://doi.org/10.1021/acs.jmedchem.6b01594.
[3] T.K. Warren, R. Jordan, M.K. Lo, A.S. Ray, R.L. Mackman, V. Soloveva, D. Siegel, M. Perron, R. Bannister, H.C. Hui, N. Larson, R. Strickley, J. Wells, K.S. Stuthman, S.A. Van Tongeren, N.L. Garza, G. Donnelly, A.C. Shurtleff, C.J. Retterer, D. Gharaibeh, R. Zamani, T. Kenny, B.P. Eaton, E. Grimes, L.S. Welch, L. Gomba, C.L. Wilhelmsen, D.K. Nichols, J.E. Nuss, E.R. Nagle, J.R. Kugelman, G. Palacios, E. Doerffler, S. Neville, E. Carra, M.O. Clarke, L. Zhang, W. Lew, B. Ross, Q. Wang, K. Chun, L. Wolfe, D. Babusis, Y. Park, K.M. Stray, I. Trancheva, J.Y. Feng, O. Barauskas, Y. Xu, P. Wong, M.R. Braun, M. Flint, L.K. McMullan, S.S. Chen, R. Fearns, S. Swaminathan, D.L. Mayers, C.F. Spiropoulou, W.A. Lee, S.T. Nichol, T. Cihlar, S. Bavari, Therapeutic efficacy of the small molecule GS-5734 against Ebola virus in rhesus monkeys, Nature 531 (2016) 381–385, https://doi.org/10.1038/nature17180.
[4] S. Mulangu, L.E. Dodd, R.T. Davey, O. Tshiani Mbaya, M. Proschan, D. Mukadi, M. Lusakibanza Manzo, D. Nzolo, A. Tshomba Oloma, A. Ibanda, R. Ali, S. Coulibaly, A.C. Levine, R. Grais, J. Diaz, H.C. Lane, J.-J. Muyembe-Tamfum, The palm writing group, A randomized, controlled trial of Ebola virus disease therapeutics, N. Engl. J. Med. 381 (2019) 2293–2303, https://doi.org/10.1056/nejmoa1910993.
[5] T.P. Sheahan, A.C. Sims, R.L. Graham, V.D. Menachery, L.E. Gralinski, J.B. Case, S.R. Leist, K. Pyrc, J.Y. Feng, I. Trantcheva, R. Bannister, Y. Park, D. Babusis, M.O. Clarke, R.L. MacKman, J.E. Spahn, C.A. Palmiotti, D. Siegel, A.S. Ray, T. Cihlar, R. Jordan, M.R. Denison, R.S. Baric, Broad-spectrum antiviral GS-5734 inhibits both epidemic and zoonotic coronaviruses, Sci. Transl. Med. 9 (2017), https://doi.org/10.1126/scitranslmed.aal3653 eaal3653.
[6] E.S. Amirian, J.K. Levy, Current knowledge about the antivirals remdesivir (GS-5734) and GS-441524 as therapeutic options for coronaviruses, One Heal 9 (2020) 1000128, https://doi.org/10.1016/j.onehlt.2020.100128.
[7] M.A. Martinez, Compounds with therapeutic potential against novel respiratory 2019 coronavirus, Antimicrob. Agents Chemother. 64 (2020), https://doi.org/10.1128/AAC.00399-20 e00399-20.
[8] T.P. Sheahan, A.C. Sims, S.R. Leist, A. Schäfer, J. Won, A.J. Brown, S.A. Montgomery, A. Hogg, D. Babusis, M.O. Clarke, J.E. Spahn, L. Bauer, S. Sellers, D. Porter, J.Y. Feng, T. Cihlar, R. Jordan, M.R. Denison, R.S. Baric, Comparative therapeutic efficacy of remdesivir and combination lopinavir, ritonavir, and tnterferon beta against MERS-CoV, Nat. Commun. 11 (2020) 222, https://doi.org/10.1038/s41467-019-13940-6.
[9] E. de Wit, F. Feldmann, J. Cronin, R. Jordan, A. Okumura, T. Thomas, D. Scott, T. Cihlar, H. Feldmann, Prophylactic and therapeutic remdesivir (GS-5734) treatment in the rhesus macaque model of MERS-CoV infection, Proc. Natl. Acad. Sci. U.S.A. 117 (2020) 6771–6776, https://doi.org/10.1073/pnas.1922083117.
[10] Remdesivir for the treatment of covid-19 — preliminary report, N. Engl. J. Med. 383 (2020) 992–994, https://doi.org/10.1056/nejmc2022236.
[11] R.T. Eastman, J.S. Roth, K.R. Brimacombe, A. Simeonov, M. Shen, S. Patnaik, M.D. Hall, Remdesivir: a review of its discovery and development leading to emergency use authorization for treatment of COVID-19, ACS Cent. Sci. 6 (2020) 672–683, https://doi.org/10.1021/acscentsci.0c00489.
[12] M. Wang, R. Cao, L. Zhang, X. Yang, J. Liu, M. Xu, Z. Shi, Z. Hu, W. Zhong, G. Xiao, Remdesivir and chloroquine effectively inhibit the recently emerged novel coronavirus (2019-nCoV) in vitro, Cell Res. 30 (2020) 269–271, https://doi.org/10.1038/s41422-020-0282-0.
[13] A.J. Pruijssers, A.S. George, A. Schäfer, S.R. Leist, L.E. Gralinksi, K.H. Dinnon, B.L. Yount, M.L. Agostini, L.J. Stevens, J.D. Chappell, X. Lu, T.M. Hughes, K. Gully, D.R. Martinez, A.J. Brown, R.L. Graham, J.K. Perry, V. Du Pont, J. Pitts, B. Ma, D. Babusis, E. Murakami, J.Y. Feng, J.P. Bilello, D.P. Porter, T. Cihlar, R.S. Baric, M.R. Denison, T.P. Sheahan, Remdesivir inhibits SARS-CoV-2 in human lung cells and chimeric SARS-CoV expressing the SARS-CoV-2 RNA polymerase in mice, Cell Rep. 32 (2020) 107940, https://doi.org/10.1016/j.celrep.2020.107940.
[14] M.L. Agostini, E.L. Andres, A.C. Sims, R.L. Graham, T.P. Sheahan, X. Lu, E.C. Smith, J.B. Case, J.Y. Feng, R. Jordan, A.S. Ray, T. Cihlar, D. Siegel, R.L. Mackman, M.O. Clarke, R.S. Baric, M.R. Denison, Coronavirus susceptibility to the antiviral remdesivir (GS-5734) is mediated by the viral polymerase and the proofreading exoribonuclease, mBio 9 (2018), https://doi.org/10.1128/mBio.00221-18 e00221-18.
[15] S.C.J. Jorgensen, R. Kebriaei, L.D. Dresser, Remdesivir: review of pharmacology, pre-clinical data, and emerging clinical experience for COVID-19, Pharmacotherapy 40 (2020) 659–671, https://doi.org/10.1002/phar.2429.
[16] C.J. Gordon, E.P. Tchesnokov, E. Woolner, J.K. Perry, J.Y. Feng, D.P. Porter, M. Götte, Remdesivir is a direct-acting antiviral that inhibits RNA-dependent RNA polymerase from severe acute respiratory syndrome coronavirus 2 with high potency, J. Biol. Chem. 295 (2020) 6785–6797, https://doi.org/10.1074/jbc.RA120.013679.
[17] K. Parang, L.I. Wiebe, E.E. Knaus, J.S. Huang, D.L. Tyrrell, In vitro anti-hepatitis B virus activities of 5′-O-myristoyl analogue derivatives of 3-fluoro-2′,3′-dideoxythymidine (FLT) and 3′-azido-2′,3′-dideoxythymidine (AZT), J. Pharm. Pharmaceut. Sci. 1 (1998) 108–114.
[18] H.K. Agarwal, G.F. Doncel, K. Parang, Synthesis and anti-HIV activities of phosphate triester derivatives of 3′-fluoro-2′,3′-dideoxythymidine and 3′-azido-2′,3′-dideoxythymidine, Tetrahedron Lett. 49 (2008) 4905–4907, https://doi.org/10.1016/j.tetlet.2008.05.149.
[19] H.K. Agarwal, K. Loethan, D. Mandal, G.F. Doncel, K. Parang, Synthesis and biological evaluation of fatty acyl ester derivatives of 2′,3′-didehydro-2′,3′-dideoxythymidine, Bioorg. Med. Chem. Lett 21 (2011) 1917–1921, https://doi.org/10.1016/j.bmcl.2011.02.070.
[20] H.K. Agarwal, B.S. Chhikara, S. Bhavaraju, D. Mandal, G.F. Doncel, K. Parang,

Emtricitabine prodrugs with improved anti-HIV activity and cellular uptake, Mol. Pharm. 10 (2013) 467–476, https://doi.org/10.1021/mp300361a.
[21] H.K. Agarwal, B.S. Chhikara, M.J. Hanley, G. Ye, G.F. Doncel, K. Parang, Synthesis and biological evaluation of fatty acyl ester derivatives of (-)-2′,3′-Dideoxy-3′-Thiacytidine, J. Med. Chem. 55 (2012) 4861–4871, https://doi.org/10.1021/jm300492q.
[22] I.M. Ibrahim, A.N. Bade, Z. Lin, D. Soni, M. Wojtkiewicz, B.L.D. Shetty, N. Gautam, J.M. McMillan, Y. Alnouti, B.J. Edagwa, H.E. Gendelman, Synthesis and characterization of a long-acting emtricitabine prodrug nanoformulation, Int. J. Nanomed. 14 (2019) 6231–6247, https://doi.org/10.2147/IJN.S215447.
[23] W. Wang, N. Smith, E. Makarov, Y. Sun, C.L. Gebhart, M. Ganesan, N.A. Osna, H.E. Gendelman, B.J. Edagwa, L.Y. Poluektova, A long-acting 3TC ProTide nanoformulation suppresses HBV replication in humanized mice, Nanomed. Nanotechnol. Biol. Med. 28 (2020) 102185, https://doi.org/10.1016/j.nano.2020.102185.
[24] R.L. Creighton, I.T. Suydam, M.E. Ebner, W.E. Afunugo, A.M. Bever, S. Cao, Y. Jiang, K.A. Woodrow, Sustained intracellular raltegravir depots generated with prodrugs designed for nanoparticle delivery, ACS Biomater. Sci. Eng. 5 (2019) 4013–4022, https://doi.org/10.1021/acsbiomaterials.9b00658.
[25] A.S. Ray, M.W. Fordyce, M.J.M. Hitchcock, Tenofovir alafenamide: a novel prodrug of tenofovir for the treatment of human immunodeficiency virus, Antivir. Res. 125 (2016) 63–70, https://doi.org/10.1016/j.antiviral.2015.11.009.
[26] A.C. Savage, L.M. Tatham, M. Siccardi, T. Scott, M. Vourvahis, A. Clark, S.P. Rannard, A. Owen, Improving maraviroc oral bioavailability by formation of solid drug nanoparticles, Eur. J. Pharm. Biopharm. 138 (2019) 30–36, https://doi.org/10.1016/j.ejpb.2018.05.015.
[27] N.J. Liptrott, M. Giardiello, T.O. McDonald, S.P. Rannard, A. Owen, Assessment of interactions of efavirenz solid drug nanoparticles with human immunological and haematological systems, J. Nanobiotechnol. 16 (2018) 22, https://doi.org/10.1186/s12951-018-0349-y.
[28] R.T. Schooley, A.F. Carlin, J.R. Beadle, N. Valiaeva, X.Q. Zhang, A.E. Clark, R.E. McMillan, S.L. Leibel, R.N. McVicar, J. Xie, A.F. Garretson, V.I. Smith, J. Murphy, K.Y. Hostetler, Rethinking Remdesivir: Synthesis, antiviral activity, and pharmacokinetics of oral lipid prodrugs, Antimicrob. Agents Chemother. 65 (2021), e0115521, https://doi.org/10.1128/AAC.01155-21.
[29] W. Yin, C. Mao, X. Luan, D.D. Shen, Q. Shen, H. Su, X. Wang, F. Zhou, W. Zhao, M. Gao, S. Chang, Y.C. Xie, G. Tian, H.W. Jiang, S.C. Tao, J. Shen, Y. Jiang, H. Jiang, Y. Xu, S. Zhang, Y. Zhang, H.E. Xu, Structural basis for inhibition of the RNA-dependent RNA polymerase from SARS-CoV-2 by remdesivir, Science 368 (2020) 1499–1504, https://doi.org/10.1126/science.abc1560.
[30] C.G. Williams, A.S. Jureka, J.A. Silvas, A.M. Nicolini, S.A. Chvatal, J. Carlson-Stevermer, J. Oki, K. Holden, C.F. Basler, Inhibitors of VPS34 and fatty-acid metabolism suppress SARS-CoV-2 replication, Cell Rep. 36 (2021), 109479, https://doi.org/10.1016/j.celrep.2021.109479.
[31] A. Watt, F. Moukambi, L. Banadyga, A. Groseth, J. Callison, A. Herwig, H. Ebihara, H. Feldmann, T. Hoenen, A novel life cycle modeling system for Ebola virus shows a genome length-dependent role of VP24 in virus infectivity, J. Virol. 88 (2014) 10511–10524, https://doi.org/10.1128/jvi.01272-14.
[32] A.S. Jureka, J.A. Silvas, C.F. Basler, Propagation, inactivation, and safety testing of SARS-CoV-2, Viruses 12 (2020) 622, https://doi.org/10.3390/v12060622.
[33] D.E. Gordon, J. Hiatt, M. Bouhaddou, V.V. Rezelj, S. Ulferts, H. Braberg, A.S. Jureka, K. Obernier, J.Z. Guo, J. Batra, R.M. Kaake, A.R. Weckstein, T.W. Owens, M. Gupta, S. Pourmal, E.W. Titus, M. Cakir, M. Soucheray, M. McGregor, Z. Cakir, G. Jang, M.J. O'Meara, T.A. Tummino, Z. Zhang, H. Foussard, A. Rojc, Y. Zhou, D. Kuchenov, R. Hüttenhain, J. Xu, M. Eckhardt, D.L. Swaney, J.M. Fabius, M. Ummadi, B. Tutuncuoglu, U. Rathore, M. Modak, P. Haas, K.M. Haas, Z.Z.C. Naing, E.H. Pulido, Y. Shi, I. Barrio-Hernandez, D. Memon, E. Petsalaki, A. Dunham, M.C. Marrero, D. Burke, C. Koh, T. Vallet, J.A. Silvas, C.M. Azumaya, C. Billesbølle, A.F. Brilot, M.G. Campbell, A. Diallo, M.S. Dickinson, D. Diwanji, N. Herrera, N. Hoppe, H.T. Kratochvil, Y. Liu, G.E. Merz, M. Moritz, H.C. Nguyen, C. Nowotny, C. Puchades, A.N. Rizo, U. Schulze-Gahmen, A.M. Smith, M. Sun, I.D. Young, J. Zhao, D. Asarnow, J. Biel, A. Bowen, J.R. Braxton, J. Chen, C.M. Chio, , U.S. Chio, I. Deshpande, L. Doan, B. Faust, S. Flores, M. Jin, K. Kim, V.L. Lam, F. Li, J. Li, Y.L. Li, Y. Li, X. Liu, M. Lo, K.E. Lopez, A.A. Melo, F.R. Moss, P. Nguyen, J. Paulino, K.I. Pawar, J.K. Peters, T.H. Pospiech, M. Safari, S. Sangwan, K. Schaefer, P.V. Thomas, A.C. Thwin, R. Trenker, E. Tse, T.K.M. Tsui, F. Wang, N. Whitis, Z. Yu, K. Zhang, Y. Zhang, F. Zhou, D. Saltzberg, A.J. Hodder, A.S. Shun-Shion, D.M. Williams, K.M. White, R. Rosales, T. Kehrer, L. Miorin, E. Moreno, A.H. Patel, S. Rihn, M.M. Khalid, A. Vallejo-Gracia, P. Fozouni, C.R. Simoneau, T.L. Roth, D. Wu, M.A. Karim, M. Ghoussaini, I. Dunham, F. Berardi, S. Weigang, M. Chazal, J. Park, J. Logue, M. McGrath, S. Weston, R. Haupt, C.J. Hastie, M. Elliott, F. Brown, K.A. Burness, E. Reid, M. Dorward, C. Johnson, S.G. Wilkinson, A. Geyer, D.M. Giesel, C. Baillie, S. Raggett, H. Leech, R. Toth, N. Goodman, K.C. Keough, A.L. Lind, R.J. Klesh, K.R. Hemphill, J. Carlson-Stevermer, J. Oki, K. Holden, T. Maures, K.S. Pollard, A. Sali, D.A. Agard, Y. Cheng, J.S. Fraser, A. Frost, N. Jura, T. Kortemme, A. Manglik, D.R. Southworth, R.M. Stroud, D.R. Alessi, P. Davies, M.B. Frieman, T. Ideker, C. Abate, N. Jouvenet, G. Kochs, B. Shoichet, M. Ott, M. Palmarini, K.M. Shokat, A. García-Sastre, J.A. Rassen, R. Grosse, O.S. Rosenberg, K.A. Verba, C.F. Basler, M. Vignuzzi, A.A. Peden, P. Beltrao, N.J. Krogan, Comparative host-coronavirus protein interaction networks reveal pan-viral disease mechanisms, Science 370 (2020) 6521, https://doi.org/10.1126/science.abe9403.
[34] M.R. Edwards, C. Pietzsch, T. Vausselin, M.L. Shaw, A. Bukreyev, C.F. Basler, High-throughput minigenome system for identifying small-molecule inhibitors of Ebola virus replication, ACS Infect. Dis. 14 (2015) 380–387, https://doi.org/10.1021/acsinfecdis.5b00053.
[35] M.R. Edwards, G. Liu, S. De, J. Sourimant, C. Pietzsch, B. Johnson, G.K. Amarasinghe, D.W. Leung, A. Bukreyev, R.K. Plemper, Z. Aron, T.L. Bowlin, D.T. Moir, C.F. Basler, Small molecule compounds that inhibit antioxidant response gene expression in an inducer-dependent manner, ACS Infect. Dis. 13 (2020) 489–502, https://doi.org/10.1021/acsinfecdis.9b00416.
[36] K. Parang, L.I. Wiebe, E.E. Knaus, J.S. Huang, D.L. Tyrrell, F. Csizmadia, In vitro antiviral activities of myristic acid analogs against human immunodeficiency and hepatitis B Viruses, Antivir. Res. 34 (1997) 75–90, https://doi.org/10.1016/S0166-3542(96)01022-4.
[37] K. Parang, E.E. Knaus, L.I. Wiebe, S. Sardari, M. Daneshtalab, F. Csizmadia, Synthesis and antifungal activities of myristic acid analogs, Arch. Pharm. (Weinheim) 329 (1996) 475–482, https://doi.org/10.1002/ardp.19963291102.
[38] K. Benson, S. Cramer, H.J. Galla, Impedance-based cell monitoring: barrier properties and beyond, Fluids Barriers CNS 10 (2013) 5, https://doi.org/10.1186/2045-8118-10-5.
[39] W.M. Schneider, J.M. Luna, H.H. Hoffmann, F.J. Sánchez-Rivera, A.A. Leal, A.W. Ashbrook, J. Le Pen, I. Ricardo-Lax, E. Michailidis, A. Peace, A.F. Stenzel, S.W. Lowe, M.R. MacDonald, C.M. Rice, J.T. Poirier, Genome-scale identification of SARS-CoV-2 and Pan-coronavirus host factor networks, Cell 184 (2021) 120–132.e14, https://doi.org/10.1016/j.cell.2020.12.006.
[40] S.T. Kang, H.C. Wang, Y.T. Yang, G.H. Kou, C.F. Lo, The DNA virus white spot syndrome virus uses an internal ribosome entry site for translation of the highly expressed nonstructural protein ICP35, J. Virol. 87 (2013) 13263–13278, https://doi.org/10.1128/JVI.01732-13.